STATISTICAL AND OVERALL UNCERTAINTIES IN BNCT MICRODOSIMETRIC MEASUREMENTS

D. Moro, E. Seravalli and P. Colautti

LNL-INFN, viale dell'Università 2. I-35020 Legnaro. Italy.

1. Introduction

In experimental microdosimetry, tissue equivalent gas proportional counters (TEPC) are used to measure pulse height spectra (then processed as microdosimetric spectra); that means ionisation event spectra generated by the radiation in a given site, which has generally 1 μm of size. The way to generate microdosimetric spectra is well described in ICRU Report 36 [1]. The microdosimetry technique can be used to measure the different dose components of a mixed radiation field [2]. Moreover, it can be used to calculate the effective biological dose [3]. Therefore, we have decided to use this technique for characterising the neutron beams that will be used for the Italian project of Boron neutron capture therapy (BNCT). In this paper we shall discuss the experimental uncertainties of the microdosimetric quantities as well as the uncertainties of the dose components measured with TEPCs. In such discussion we shall use microdosimetric spectra collected at the Tapiro reactor.

2. Microdosimetry at the TAPIRO reactor

The TAPIRO[1] fast reactor is located in the ENEA research centre called Casaccia (near Rome). It produces a fast neutron flux that has been opportunely moderated with a thermal column (see figure 1) for studying the microdosimetric features of possible BNCT[2] radiation fields.

An example of microdosimetric spectra, collected inside the irradiation box of TAPIRO thermal column is shown in figure 2. The spectra have been collected with a cylindrical TEPC, the cathode wall of which can be replaced. Measurements have been performed with cathode wall made of ordinary A-150 plastic and with cathode wall made of A-150 plastic loaded with 100 μg/g (100 ppm) of ^{10}B. In the left side of figure 2, the event frequency distributions with and without ^{10}B are plotted. More than 99.9% of events are due to electron set in motion by photons (events of size less than 12 keV/μm). The remaining events are due to proton and light ions set in motion by

[1] TAPIRO stands for: TAratura PIla Rapida potenza zerO. It is a fast nuclear reactor of 5kW power.

[2] BNCT stands for Boron Neutron Therapy Capture. This is a new promising cancer treatment technique that uses thermal (or epithermal) neutrons to irradiate tumours previously loaded with ^{10}B. Thermal neutron absorption on the ^{10}B nucleus gives rise to the production of ^{4}He and ^{7}Li; the ranges of these charge particles in tissues are as short as the diameter of the cell nucleus and consequently if tumor cells are loaded with ^{10}B all the energy is released inside the tumor cells which is killed with high probability while the neighbouring (healthy) cells are not damaged.

neutrons. The presence of 100 ppm of ^{10}B in the cathode wall gives rise to high y-value events (about 0.2% of the total) due Helium and Lithium ions emerging from the $^{10}B(n,\alpha)^{7}Li$ reaction. These events increase the yield of events of size more than 12 keV/μm.

In the right side of figure 2. the usual microdosimetric representation of the same data in a semi-logarithmic plot, where the abscissa is the logarithm of the lineal energy ***ln(y)*** [keV/μm] and the ordinate is the product ***yd(y)*** (where ***y*** is the lineal energy and ***d(y)*** is the dose-weighted distribution of ***y***. Without ^{10}B, the photon-induced events contribute 86% to the total dose. When ^{10}B is present, the few more events give rise to a high dose peak at about 300 keV/μm, which represents the 33% of the total dose. More about microdosimetric spectra at TAPIRO reactor are published elsewhere [4].

The microdosimetric spectrum is usually processed to obtain the mean values $\overline{y_f}$ (the mean lineal energy), $\overline{y_d}$ (the dose-weighted mean lineal energy) and ***RBE*** (the relative biological efficiency). The overall uncertainties of the aforementioned means, in proton beam microdosimetry, have been analysed in an other paper [5].

Figure 1 The Tapiro reactor thermal column. The TEPC is going to be inserted in the irradiation box, which is then closed with a graphite lid and graphite bars.

A microdosimetric spectrum is originally collected on three different multi channel analysers. In fact, preamplifier pulses are sent to three different linear amplifiers, which have different gains in order to have the same resolution both for small-size y-events and large-size y-events. The three original sub-spectra, calibrated in Volt, are then joined and processed to have the same number of channels per ***y*** decade (the usual number of channels is 60, but any number can be chosen).

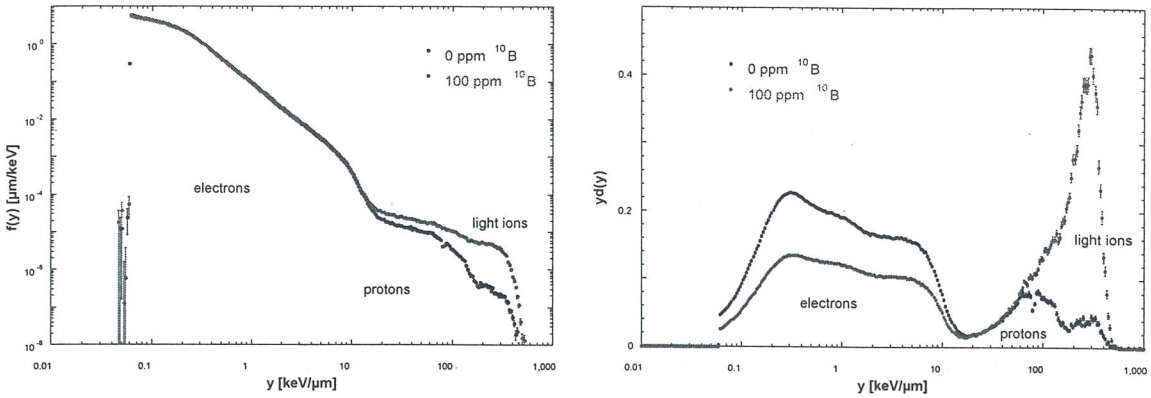

Figure 2 Microdosimetric spectra measured at the TAPIRO reactor (see text) using a normal cathode and one loaded with 100 µg/g of ^{10}B. The simulated diameter is equal to 1 µm. Left side: frequency density distributions. Right side: weighted distributions.

Therefore, any channel in a microdosimetric spectrum has the same *logarithmic size*. The full spectrum has $n(\tilde{y}) \cdot \Delta\tilde{y}$ events (measured counts divided by the acquisition dead time) per channel, where the symbol $\tilde{y}$ means that the microdosimetric spectrum has not yet been calibrated in lineal energy; therefore $\tilde{y}$ is in **V** and $\Delta\tilde{y}$ is the channel size, always in **V**. The spectrum is eventually recalibrated in lineal energy.

3. Statistical errors

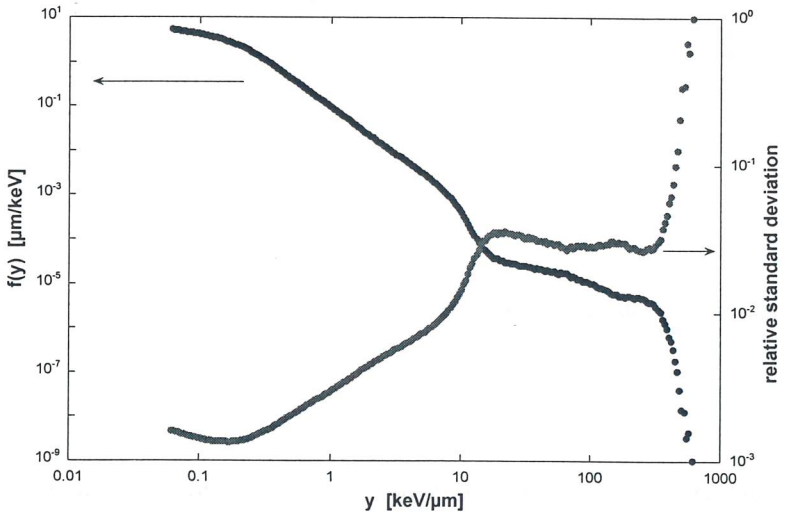

Figure 3. In blue frequency density distribution (left ordinate), measured at the TAPIRO reactor with 100 ppm of ^{10}B, and its relative uncertainty (red). The total events are 3.03e7

The event statistics of a neutron field microdosimetric spectrum varies with the lineal energy size. The statistic range is very large, since the events-rate occurrence covers almost 10 decades (see figure 3). The error bars in figure 2 are ± 1 standard deviation (SD) of the event density in any logarithmic bin. Following the Poisson statistics, 1 SD of event density in the i_{th} bin ($\sigma_{n(y_i)}$) is:

$$\sigma_{n(y_i)} = \sqrt{f(y_i)/(n \cdot \Delta y_i)} \qquad (1)$$

where $f(y_i)$ is the value of the frequency density distribution at the i_{th} bin, Δy_i is the largeness of the i_{th} bin and n is the sum of all events.

In figure 3 the relative statistical uncertainty of the frequency density distribution with 100 ppm of ^{10}B is plotted. In order to have a relative uncertainty of about 2 % in the BNC event region, more than 30 millions of events have been collected.

4. Lineal energy calibration uncertainty

In order to convert $\tilde{y}$ [V] in y [keV/μm], the pulse spectrum has to be calibrated. Waker has observed that the main source of uncertainty in microdosimetric measurements with commercial TEPCs is the lineal energy calibration performed with the internal alpha source [6]. Pihet writes that, comparing different commercial TEPCs, such uncertainty is 10% [7]. The main source of this uncertainty is the poor knowledge of the energy spectrum of the alpha particles entering the TEPC sensitive volume, as well as the poor knowledge of the alpha particle mean chord in the TEPC.

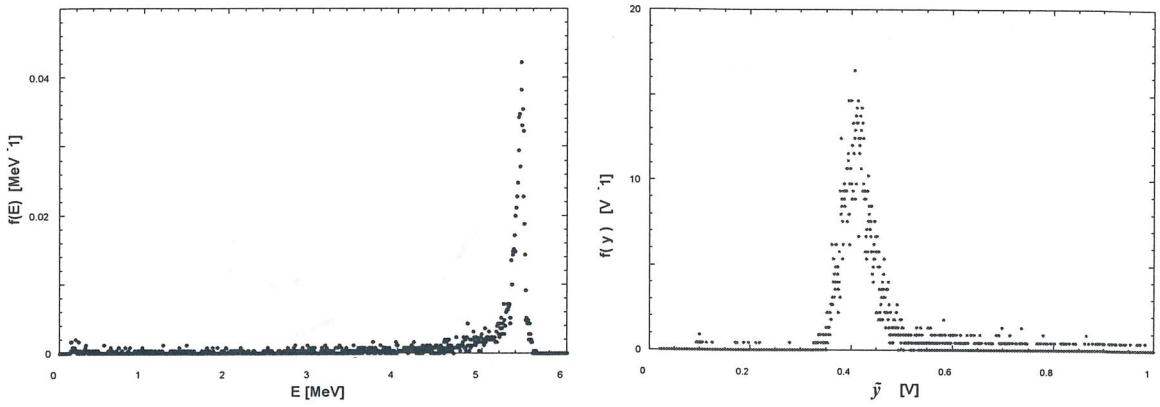

Figure 4. Energy density distribution of the internal ^{244}Cm alpha source of the TEPC used in the measurements (left side). The alpha mean energy is 4.93 MeV. Pulse height spectrum of the alpha source (right side).

The detector used for this study has a well-defined cylindrical geometry, which enables of calculating with precision the alpha path inside the detector [4, 8]. Moreover the alpha energy spectrum has been measured with precision of **0.2%** with a solid-state detector [14] (see figure 4). The α-source pulse-height spectrum, measured with the TEPC, has a relative uncertainty of **0.3%**

(acquisition system linearity uncertainty). The relative standard deviation of the alpha source (left side of figure 4) is 22%. The relative standard deviation of the pulse height spectrum (right side of figure 4) is 26%. That means the gas gain fluctuations do not increase significantly the y-value fluctuations in 1 μm site.

The calibration statistical uncertainty can be minimised. The counter gas is continuously flown, the pressure measured with high precision and no anode wire aging has been observed. Therefore the gas gain is constant. When the alpha calibration is used, the calibration uncertainty is therefore mainly due to the uncertainty in the stopping power tables used. Moreover there is the error in the use of a constant W-value (in particular the W-value for alpha particles) to calibrate a spectrum due to events of energy deposits caused by different particles (electrons, protons…).

The relative uncertainty of the range-energy tables used to estimate the energy lost by alpha particles in the sensitive volume of the TEPC is 5 % [9]. This error is mainly due to systematic rather than statistical errors. It is, therefore, questionable whether the concept of standard deviation is applicable. However, if one wants to follow the recommendations of CIPM [10], also given in Giacomo [11], then the systematic uncertainty is converted to "standard deviation" by multiplying it by factor of 0.5 [9]. In this way this uncertainty can be used in the error propagation formula.

The relative uncertainty due to the use of a constant W-value is estimated equal to 1.5 %, following the suggestions of J.Burmeister [12]. The uncertainty of the δ-ray escape calculation is **1%** in 1 μm site. Finally there is the statistical uncertainty of the alfa source pulse-height spectrum, which is, in our case, 0.82%. Therefore the relative uncertainty, which affects the calibration procedure with the internal alpha source is **3.2%**, i.e. the squared root of the sum of: 2.5%, 1.5%, 1% and 0.82%.

Microdosimetric spectra can be self-calibrated by using the so-called electron edge, proton edge, alpha edge. These edges are located at the maximum pulse size that respectively electrons, protons and alpha particle can give rise. The maximum pulse size occurs when the charged particle exactly stops at the end of the TEPC's sensitive volume, after having crossed it along the main sensitive volume chord.

In figure 5, five microdosimetric spectra, calibrated with the internal alpha source, are plotted together with the second derivative of $\Delta y \cdot y \cdot n(y)$, that means the not-normalised values of $yd(y)$. The spectra have been collected with different ^{10}B content in the counter. The second derivative of a microdosimetric spectrum shows local maxima where the spectrum slope changes positively. In figure 5, 3 local maxima are plotted. They are close, but not exactly at, the electron

edge, proton edge and alpha edge. The physical reason of these maxima lays in the stopping of the relative decreasing of the dose contribution with the finishing of the events due to a given charged particle. After the particle edge, the yd(y) distribution decreases less steeply or increases more sharply; in both the case that produces a local maximum in the second derivatives. Depending on the event statistics of the exact stoppers which give rise to the edge and on the population of events after the edge, the local maximum can be more or less sharp and more or less shifted towards y-values higher than the edge.

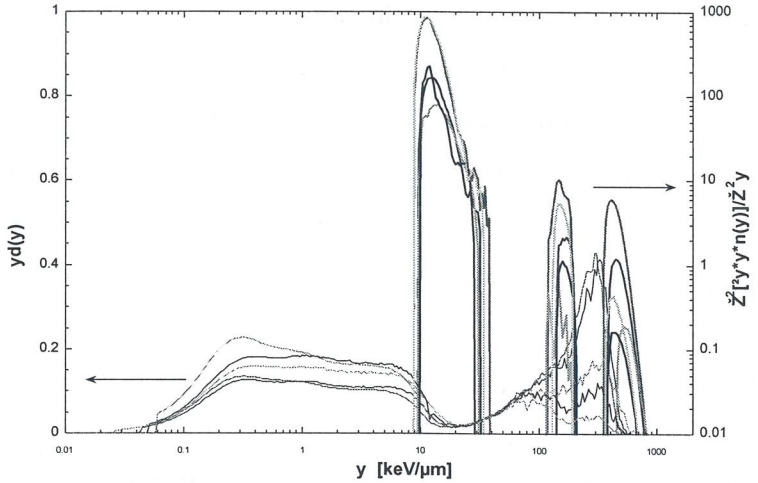

Figure 5. Microdosimetric spectra (1 µm diametre) measured at TAPIRO reactor with different ^{10}B contents and the spectrum second derivatives. To facilitate the reading the second derivatives outside the region of interest have been cancelled (see text).

In figure 5, the second derivative local maxima are plotted, while the second derivative has been cancelled everywhere else to simplify the plot observation. In table 1 the second-derivative local maximum values are reported.

Table 1. Position of the three second-derivative local maxima of figure 5 and the position precision.

	Local maximum position [keV/µm]	Relative standard deviation %
1st maximum	12.2 ± 1.0	8.4
2nd maximum	155.5 ± 6.5	4.2
3rd maximum	447 ± 50	11.2

The position of the second-derivative local maxima depends more or less on the spectrum shape. This dependence is minimised for the 2nd local maximum, close to the proton edge, which has a position rather independent on the ^{10}B content. It can be used as lineal energy calibration

reference ascertained the event statistics is large enough to eliminate the spurious second-derivative fluctuations, which decrease the maximum localisation precision.

A more precise lineal energy calibration can be performed with pure photon beams.

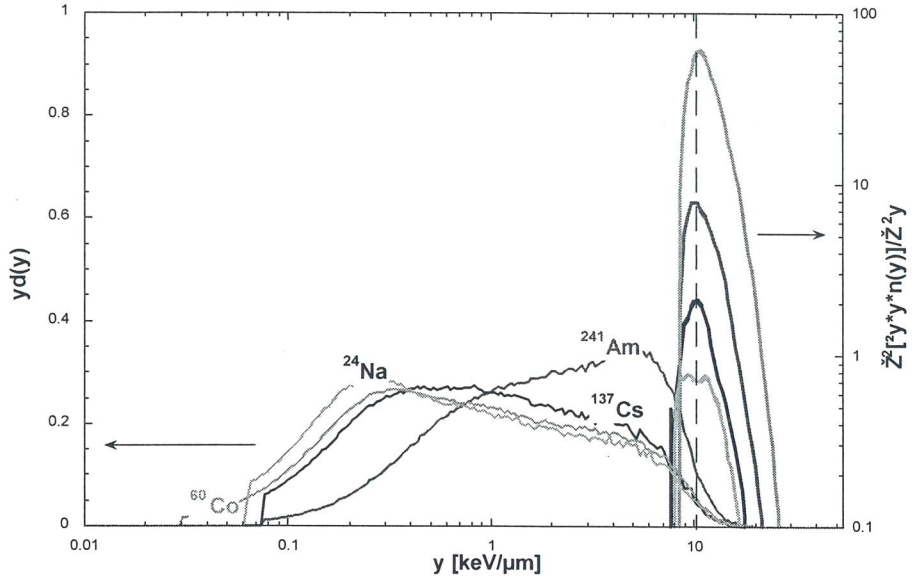

Figure 6. Microdosimetric spectra (1 μm diameter) of different gamma sources and the spectrum second derivatives. To facilitate the reading the second derivatives outside the region of interest have been cancelled (see text). The vertical dashed line points out the mean value of the second-derivative maximum position.

The microdosimetric spectra of four gamma sources have been measured and the second derivative of the spectra have been calculated. The gamma energies are: 59.5 keV (^{241}Am), 662 keV (^{137}Cs), 1250 keV (^{60}Co) and 2754 keV (^{24}Na). The second derivative shows a clear local maximum near the electron edge. In figure 6 microdosimetric spectra, calibrated with the internal alpha source, and the second-derivative local maxima are plotted together. The second derivative for other y-values have been cancelled to facilitate the plot reading. Figure 6 shows that in spite of the very different photon energies, the second-derivative local maximum position is rather stable: 10.2 ± 0.37 keV/μm. With respect the 2nd maximum of figure 5, this maximum position is more precise and easier to measure by using some intense external photon source of any energy. This "electron edge" calibration has relative standard deviation of **3.6%**.

Pay attention that this "electron edge" calibration has been calibrated with the alpha calibration. Therefore, the electron edge calibration overall uncertainty is **4.8%** (the 3.2% of alpha-calibration uncertainty has been added). For using this calibration for photon microdosimetric spectra, it has to be corrected by the ratio of the energy per ion pair production W_e/W_α, whose value for Propane-TE gas mixture is 0.964 ± 0.036.

Note that the "electron edge" position is significantly depending on the site diameter [8], namely on the gas pressure. The value 10.2 keV/μm is valid only for 1 μm simulated site. This value increases decreasing the gas pressure. Therefore, the "electron edge" method is not advised when the gas pressure in the counter is not properly measured.

5. Spectrum extrapolation uncertainty

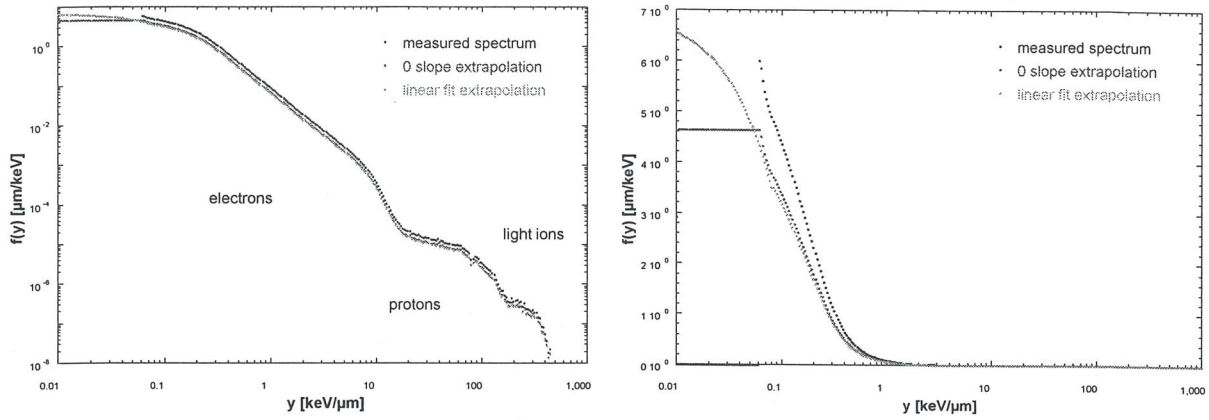

Figure 7. Measured frequency density distribution and extrapolated distributions. Details of two possible extrapolation ways (right side of the figure) and consequential changes of the full distribution (left side of the figure).

TEPCs have a lower detection threshold, the value of which depends on the electronic noise and on the counter gas gain. In other words, TEPC detection efficiency is not 100%, because they do not measure all the ionisation events which take place in their sensitive volume. Therefore, in order to use microdosimetric spectra for quantitative dosimetry, it is necessary to extrapolate the measured spectra down to one ionisation event (on average). We have chosen to extrapolate linearly the last part of the pulse-height frequency spectrum down to the $\tilde{y}_{\min}$-value, which becomes, after the lineal energy calibration, to 0.01 keV/μm. In the figure 7 spectrum, the noise-free detection threshold is 0.08 keV/μm. That means the **event-detection efficiency is 68%.** However, the lost events (32%) are very small. Therefore, the **dose-detection efficiency is 96%.**

The event frequency extrapolation is always rather arbitrary. Therefore, we have chosen of considering all the extrapolated part as a systematic uncertainty (in following processed as a standard deviation dividing by 2 the systematic uncertainty [9]). The extrapolation-due error in a microdosimetric calculated means is therefore assumed to be half of the mean value calculated from $\tilde{y}_{\min}$ and $\tilde{y}_{thr}$, where $\tilde{y}_{thr}$ is the lower detection threshold value.

6. Weighting function uncertainty

Although the relative biological effectiveness (***RBE***) is a radiobiological measurement, microdosimetric experimental data can be used to assess the ***RBE*** by using the following equation:

$$RBE = \sum_{0.01}^{y_{max}} r(y_i) \cdot d(y_i) \cdot \Delta y_i \qquad (2)$$

$d(y_i)$ is the dose-weighted probability density at y_i and the index i runs along all the measured and extrapolated channels. $r(y)$ is an empirical weighting function (see figure 8) extracted by as system of aforementioned equations, where different ***RBE*** values have been measured in different radiation fields. ***RBE*** values have been measured by the radiobiologists and $d(y)$ by physicists. $r(y)$ depends on the biological endpoint, on the absorbed dose at which the ***RBE*** values were measured and on the microdosimetric spectra site diameter. We have used the weighting function published by Pihet et al. [13], which was calculated from radiobiological ***RBE*** values for early effects in mice at 8 Gy and microdosimetric spectra in 2 μm site [13]. We have assumed that the spectra differences between 2 μm and 1 μm sites are negligible and applied the weighting function of figure 8 to 1 μm site size spectra. The r(y) uncertainty (± 1 SD) depends on the y-value. Moreover, it is not symmetric (+1SD ≠ -1SD). In figure 8 is plotted the maximum uncertainty for any y-value.

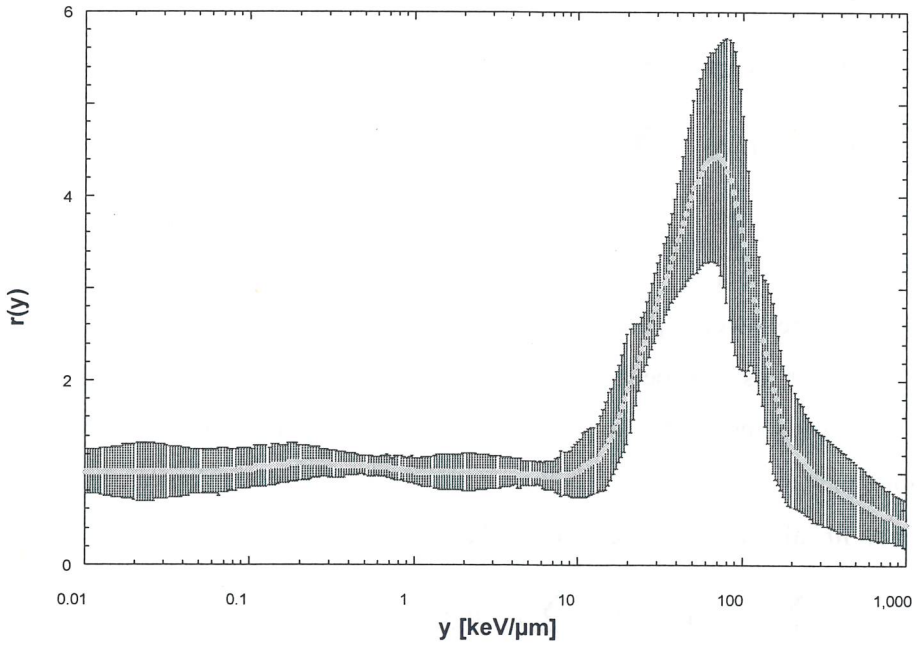

Figure 8. Weighting function of the density probability function $d(y)$ in 2 μm of size to obtain ***RBE*** of early intestine damage in mice at 8 Gy (thick yellow line) and its maximum uncertainty ± 1 SD [13] (red bars).

r(y) value is 1 up to 10 keV/μm, it reaches a maximum of 4.5 at about 70 keV/μm and becomes less than 1 for y-values larger than 250 keV/μm. This last fact is interpreted as an over-killing effect of very large y-values The accuracy of ***r(y)*** depends on the y-value, being rather low for y-values more than about 250 keV/μm

The uncertainties plotted in figure 8 are not symmetric, being +SD ≠ -SD. Therefore in the following, for calculating the overall ***RBE*** uncertainty, we will take the maximum SD value at any point (SD_{max}) and substituted the uncertainties of figure 8 with ± SD_{max}

7. Overall uncertainty of $\overline{y_f}$

The mean lineal energy of the discreet stochastic variable y is:

$$\overline{y_f} = \sum_{0.01}^{y_{max}} y_i \cdot f(y_i) \cdot \Delta y_i \qquad (3)$$

where y_{max} is the maximum of lineal energy of microdosimetric spectrum (in keV/μm) and 0.01 (in keV/μm) is the minimum value at which we extrapolate the frequency spectrum. $f(y_i)$ is the density probability of the y_i-value, which has been counted $n(y_i) \cdot \Delta y_i$ times:

$$f(y_i) = \frac{n(y_i)}{\sum_{0.01}^{y_{max}} n(y_i) \cdot \Delta y_i} \qquad (4)$$

By substituting $f(y_i)$ with the equation (3) and by splitting the equation in a sum of two terms:

$$\overline{y_f} = \frac{\sum_{0.01}^{y_{thr}} y_i \cdot n(y_i) \cdot \Delta y_i + \sum_{y_{thr}}^{y_{max}} y_i \cdot n(y_i) \cdot \Delta y_i}{\sum_{0.01}^{y_{max}} n(y_i) \cdot \Delta y_i} \qquad (4)$$

where y_{thr} is the lower experimental threshold value.

However, as said before, spectra are first processed in Volts and then calibrated in lineal energy by using the calibration factor F_{cal}, which has dimensions keV·V^{-1}·μm^{-1}. By changing the variable $y_i = F_{cal} \cdot \tilde{y}_i$, where $\tilde{y}$ is the y-value in V, and remembering that $n(y_i) \cdot \Delta y_i = n(\tilde{y}_i) \cdot \Delta \tilde{y}_i$, the mean lineal energy can be expressed as:

$$\overline{y_f} = F_{cal} \cdot \frac{\sum_{\tilde{y}_{min}}^{\tilde{y}_{thr}} \tilde{y}_i \cdot n(\tilde{y}_i) \cdot \Delta \tilde{y}_i + \sum_{\tilde{y}_{thr}}^{\tilde{y}_{max}} \tilde{y}_i \cdot n(\tilde{y}_i) \cdot \Delta \tilde{y}_i}{\sum_{\tilde{y}_{min}}^{\tilde{y}_{max}} n(\tilde{y}_i) \cdot \Delta \tilde{y}_i} \qquad (5)$$

From the error propagation formula we can obtain the $\overline{y_f}$ relative error:

$$\left(\frac{\sigma_{\overline{y_f}}}{\overline{y_f}}\right)^2 = \left(\frac{\sigma_{F_{cal}}}{F_{cal}}\right)^2 + \left(\frac{\sigma_\Sigma}{\Sigma}\right)^2 \qquad (6)$$

where the symbol $\sum$ represents the second factor of the right side of the equation (5).

It is no easy to calculate $\left(\frac{\sigma_\Sigma}{\Sigma}\right)$, since numerator and denominator of $\sum$ are correlated and therefore:

$$\left(\frac{\sigma_\Sigma}{\Sigma}\right)^2 = \left(\frac{\sigma_{num}}{num}\right)^2 + \left(\frac{\sigma_{den}}{den}\right)^2 + 2\cdot\sigma_{num}\cdot\sigma_{den}\cdot\rho_{corr} \qquad (7)$$

where *num* and *den* are respectively the numerator and denominator of $\sum$ whilst ρ_{corr} is the correlation coefficient between numerator and denominator. It is simple to demonstrate that this correlation is negative; that is numerator fluctuations give rise to fluctuation of the same sign at the denominator and consequently the ratio presents a smaller fluctuation. Therefore, if we assume $\rho_{corr}=0$ we overestimate the error.

The error of $\tilde{y}_i$ depends on the *integral linearity* of the electronic chains and the error of $\Delta\tilde{y}_i$ depends on the *differential linearity* of the electronic chains. Before any measurement, both the integral and differential electronic chain linearity are measured with a precise pulse generator and a ramp generator. Microdosimetric measurements are performed only if both the electron chain linearities are good. Therefore, we can disregard the errors on both $\tilde{y}_i$ and $\Delta\tilde{y}_i$.

The error of $\sum$ numerator, σ_{num}, is the sum of two contributes:

$$\sigma_{num}^2 = \sigma_{extr}^2 + \sigma_{meas}^2 \qquad (8)$$

therefore:

$$\left(\frac{\sigma_{\overline{y_f}}}{\overline{y_f}}\right)^2 = \left(\frac{\sigma_{F_{cal}}}{F_{cal}}\right)^2 + \left(\frac{\sigma_{extr}}{num}\right)^2 + \left(\frac{\sigma_{meas}}{num}\right)^2 + \left(\frac{\sigma_{den}}{den}\right)^2 \qquad (9)$$

where σ_{extr} is the uncertainty of the extrapolation part and σ_{meas} the uncertainty of the measured part of the spectrum. According to the paragraph 5 we have:

$$\sigma_{extr}^2 = \left(0.5\cdot\sum_{\tilde{y}\,\min}^{\tilde{y}_{thr}}\tilde{y}_i\cdot n(\tilde{y}_i)\cdot\Delta\tilde{y}_i\right)^2 \qquad (10)$$

where $n(\tilde{y}_i)$ are the event linearly extrapolated by best fitting the last measured points.

σ_{meas} depends only on the fluctuations of $n(\tilde{y}_i)$, since we have assumed that $\tilde{y}_i$ and $\Delta\tilde{y}_i$ have not error. Taking into account that the uncertainty of events of the i^{th} interval is the events number

squared root, that the events of i[th] interval the are $n(\tilde{y}_i)\cdot\Delta\tilde{y}_i$ and the squared standard deviation of a sum is the sum of addenda squared standard deviations:

$$\sigma^2_{meas} = \sum_{\tilde{y}_{thr}}^{\tilde{y}_{max}} \tilde{y}_i^{\,2}\cdot\Delta\tilde{y}_i\cdot n(\tilde{y}_i) \tag{11}$$

The quadratic error of the denominator, σ_{den}, is the sum of the quadratic errors of denominator addenda, where the sum runs over all the y-value range. However, we consider only the uncertainties on the experimental data, since the extrapolated events are usually very large, masking the fluctuations due to the real measured data. Therefore the sum is performed only on the measured y-values.

$$\frac{\sigma^2_{den}}{den^2} = \frac{\sum_{\tilde{y}_{thr}}^{\tilde{y}_{max}}\Delta\tilde{y}_i\cdot n(\tilde{y}_i)}{\left(\sum_{\tilde{y}_{thr}}^{\tilde{y}_{max}}\Delta\tilde{y}_i\cdot n(\tilde{y}_i)\right)^2} \tag{12}$$

Substituting all the components of equation 9, we obtain the relative error of $\overline{y_f}$:

$$\left(\frac{\sigma_{\overline{y_f}}}{\overline{y_f}}\right)^2 = \left(\frac{\sigma_{F_{cal}}}{F_{cal}}\right)^2 + \frac{\left(0.5\cdot\sum_{\tilde{y}\,\min}^{\tilde{y}_{thr}}\tilde{y}_i\cdot n(\tilde{y}_i)\cdot\Delta\tilde{y}_i\right)^2}{\left(\sum_{\tilde{y}\,\min}^{\tilde{y}_{max}}\tilde{y}_i\cdot n(\tilde{y}_i)\cdot\Delta\tilde{y}_i\right)^2} + \frac{\sum_{\tilde{y}_{thr}}^{\tilde{y}_{max}}\tilde{y}_i^{\,2}\cdot\Delta\tilde{y}_i\cdot n(\tilde{y}_i)}{\left(\sum_{\tilde{y}\,\min}^{\tilde{y}_{max}}\tilde{y}_i\cdot n(\tilde{y}_i)\cdot\Delta\tilde{y}_i\right)^2} + \frac{\sum_{\tilde{y}_{thr}}^{\tilde{y}_{max}}\Delta\tilde{y}_i\cdot n(\tilde{y}_i)}{\left(\sum_{\tilde{y}_{thr}}^{\tilde{y}_{max}}\Delta\tilde{y}_i\cdot n(\tilde{y}_i)\right)^2} \tag{13}$$

By substituting again $\tilde{y} = y / F_{cal}$, the relative overall error of $\overline{y_f}$ can be also written:

$$\left(\frac{\sigma_{\overline{y_f}}}{\overline{y_f}}\right)^2 = \left(\frac{\sigma_{F_{cal}}}{F_{cal}}\right)^2 + \frac{\left(0.5\cdot\sum_{0.01}^{y_{thr}}y_i\cdot n(y_i)\cdot\Delta y_i\right)^2}{\left(\sum_{0.01}^{y_{max}}y_i\cdot n(y_i)\cdot\Delta y_i\right)^2} + \frac{\sum_{y_{thr}}^{y_{max}}y_i^{\,2}\cdot\Delta y_i\cdot n(y_i)}{\left(\sum_{0.01}^{y_{max}}y_i\cdot n(y_i)\cdot\Delta y_i\right)^2} + \frac{\sum_{y_{thr}}^{y_{max}}\Delta y_i\cdot n(y_i)}{\left(\sum_{y_{thr}}^{y_{max}}\Delta y_i\cdot n(y_i)\right)^2} \tag{14}$$

By remembering that $n(y_i)=n\,f(y_i)$ where $f(y_i)$ is the value of the probability density function at y_i and n is the sum of all the measured events and changing the lower sum limit in the denominator of the 3[rd] addendum (in such a way the 3[rd] addendum value will be bigger than that one it ought to be), the relative uncertainty can written as function of $f(y)$:

$$\left(\frac{\sigma_{\overline{y_f}}}{\overline{y_f}}\right)^2 < \left(\frac{\sigma_{F_{cal}}}{F_{cal}}\right)^2 + \frac{\left(0.5\cdot\sum_{0.01}^{y_{thr}} y_i\cdot f(y_i)\cdot\Delta y_i\right)^2}{\left(\sum_{0.01}^{y_{max}} y_i\cdot f(y_i)\cdot\Delta y_i\right)^2} + \frac{\sum_{y_{thr}}^{y_{max}} y_i^{\,2}\cdot f(y_i)\cdot\Delta y_i}{n\cdot\left(\sum_{y_{thr}}^{y_{max}} y_i\cdot f(y_i)\cdot\Delta y_i\right)^2} + \frac{1}{n\cdot\sum_{y_{thr}}^{y_{max}} f(y_i)\cdot\Delta y_i} \quad (15)$$

Where the ratio σ_{Fcal}/F_{cal} value is 0.048 when the lineal energy calibration is made with the electron edge of a pure photon field (see paragraph 4).

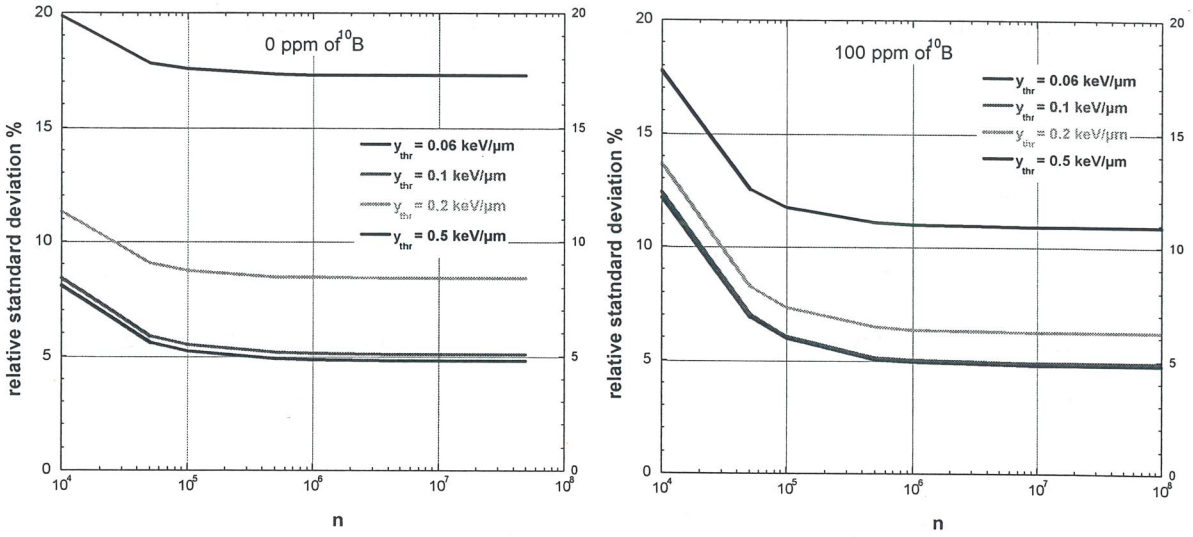

Figure 9. $\overline{y_f}$ relative overall uncertainty (1 SD) against measured events with different lower detection thresholds. Left side: spectrum without ^{10}B. Right side: spectrum with 100 ppm of ^{10}B.

In figure 9 the $\overline{y_f}$ relative overall uncertainties of the two spectra of figure 2 are plotted against total events and for different lower detection thresholds. Figure 9 shows that with a lower detection threshold of 0.1 keV/µm and 10^6 events the overall uncertainty of $\overline{y_f}$ is nearly 5%, both when 0 ppm of ^{10}B is added and when 100 ppm of ^{10}B are

added. These values are close to the lineal calibration uncertainty. There is not significant advantage to reduce the lower detection threshold at values less than 0.1 keV/µm. Similarly, there is not significant advantage to have more the 10^6 events. On the contrary, less total events and higher values of the lower detection threshold increase the $\overline{y_f}$ uncertainty

8. Overall uncertainty of $\overline{y_d}$

The lineal energy weighted-mean of the discreet stochastic variable y is:

$$\overline{y_d} = \sum_{0.01}^{y_{max}} y_i \cdot d(y_i) \cdot \Delta y_i \tag{16}$$

where y_{max} is the maximum of lineal energy of microdosimetric spectrum (in keV/μm) and 0.01 (in keV/μm) is the minimum value at which we extrapolate the frequency spectrum. $d_i(y)$ is the dose-weighted probability density of the y_i-value, which has been counted $n(y_i) \cdot \Delta y_i$ times:

$$d(y_i) = \frac{y_i \cdot n(y_i)}{\sum_{0.01}^{y_{max}} y_i \cdot n(y_i) \Delta y_i} \tag{17}$$

By substituting (in 16) $d(y_i)$ with the equation 17 and by splitting the equation in a sum of two terms:

$$\overline{y_d} = \frac{\sum_{0.01}^{y_{thr}} y_i^2 \cdot n(y_i) \cdot \Delta y_i + \sum_{y_{thr}}^{y_{max}} y_i^2 \cdot n(y_i) \cdot \Delta y_i}{\sum_{0.01}^{y_{max}} y_i \cdot n(y_i) \cdot \Delta y_i} \tag{18}$$

where y_{thr} is the low experimental threshold. Similarly to that done for $\overline{y_f}$, the calibration factor can be extracted out the sums. Therefore, the dose-weighted mean lineal energy can be expressed as:

$$\overline{y_d} = F_{cal} \cdot \frac{\sum_{\tilde{y}_{min}}^{\tilde{y}_{thr}} \tilde{y}_i^2 \cdot n(\tilde{y}_i) \cdot \Delta \tilde{y}_i + \sum_{\tilde{y}_{thr}}^{\tilde{y}_{max}} \tilde{y}_i^2 \cdot n(\tilde{y}_i) \cdot \Delta \tilde{y}_i}{\sum_{\tilde{y}_{min}}^{\tilde{y}_{max}} \tilde{y}_i \cdot n(\tilde{y}_i) \cdot \Delta \tilde{y}_i} \tag{19}$$

where $\tilde{y}$ is the y-value in V and $F_{cal}\,[keV \cdot \mu m^{-1} \cdot V^{-1}] = y / \tilde{y}$.

From the error propagation formula:

$$\left(\frac{\sigma_{\overline{y_d}}}{\overline{y_d}}\right)^2 = \left(\frac{\sigma_{F_{cal}}}{F_{cal}}\right)^2 + \left(\frac{\sigma_{\Sigma}}{\Sigma}\right)^2 \tag{20}$$

where $\sum$ is the second factor of the right side of equation 19. And then:

$$\left(\frac{\sigma_{\overline{y_d}}}{\overline{y_d}}\right)^2 = \left(\frac{\sigma_{F_{cal}}}{F_{cal}}\right)^2 + \left(\frac{\sigma_{extr}}{num}\right)^2 + \left(\frac{\sigma_{meas}}{num}\right)^2 + \left(\frac{\sigma_{den}}{den}\right)^2 \tag{21}$$

By using the same considerations used for $\overline{y_f}$, the $\overline{y_d}$ overall relative uncertainty is:

$$\left(\frac{\sigma_{\overline{y_d}}}{\overline{y_d}}\right)^2 = \left(\frac{\sigma_{F_{cal}}}{F_{cal}}\right)^2 + \frac{\left(0.5\cdot\sum_{\tilde{y}_{\min}}^{\tilde{y}_{thr}}\tilde{y}_i^2\cdot n(\tilde{y}_i)\cdot\Delta\tilde{y}_i\right)^2}{\left(\sum_{\tilde{y}_{\min}}^{\tilde{y}_{\max}}\tilde{y}_i^2\cdot n(\tilde{y}_i)\cdot\Delta\tilde{y}_i\right)^2} + \frac{\sum_{\tilde{y}_{thr}}^{\tilde{y}_{\max}}\tilde{y}_i^4\cdot\Delta\tilde{y}_i\cdot n(\tilde{y}_i)}{\left(\sum_{\tilde{y}_{\min}}^{\tilde{y}_{\max}}\tilde{y}_i^2\cdot n(\tilde{y}_i)\cdot\Delta\tilde{y}_i\right)^2} + \frac{\sum_{\tilde{y}_{thr}}^{\tilde{y}_{\max}}\tilde{y}_i^2\cdot\Delta\tilde{y}_i\cdot n(\tilde{y}_i)}{\left(\sum_{\tilde{y}_{thr}}^{\tilde{y}_{\max}}\tilde{y}_i\cdot\Delta\tilde{y}_i\cdot n(\tilde{y}_i)\right)^2} \quad (22)$$

By substituting again $\tilde{y} = y / F_{cal}$, the relative overall error of $\overline{y_d}$ can be also written:

$$\left(\frac{\sigma_{\overline{y_d}}}{\overline{y_d}}\right)^2 = \left(\frac{\sigma_{F_{cal}}}{F_{cal}}\right)^2 + \frac{\left(0.5\cdot\sum_{0.01}^{y_{thr}}y_i^2\cdot n(y_i)\cdot\Delta y_i\right)^2}{\left(\sum_{0.01}^{y_{\max}}y_i^2\cdot n(y_i)\cdot\Delta y_i\right)^2} + \frac{\sum_{y_{thr}}^{y_{\max}}y_i^4\cdot\Delta y_i\cdot n(y_i)}{\left(\sum_{0.01}^{y_{\max}}y_i^2\cdot n(y_i)\cdot\Delta y_i\right)^2} + \frac{\sum_{y_{thr}}^{y_{\max}}y_i^2\cdot\Delta y_i\cdot n(y_i)}{\left(\sum_{y_{thr}}^{y_{\max}}y_i\cdot\Delta y_i\cdot n(y_i)\right)^2} \quad (23)$$

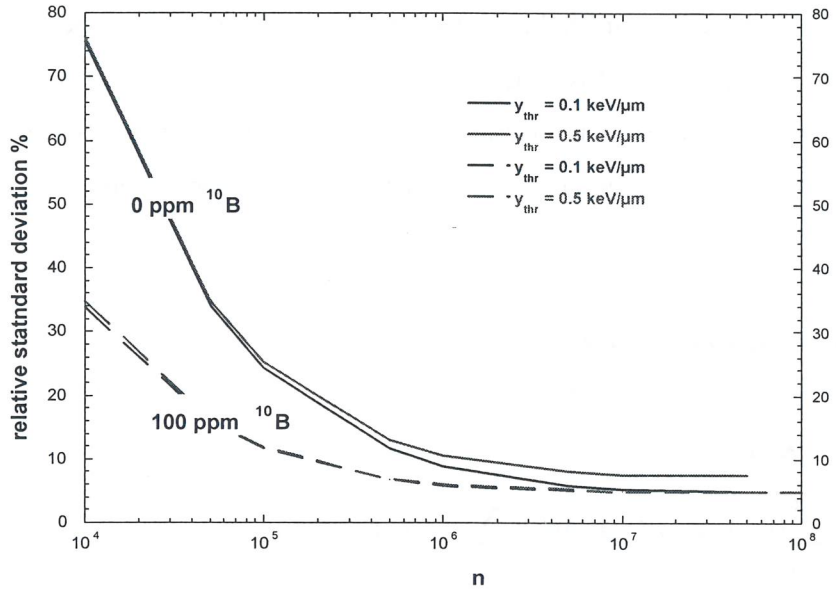

Figure 10. $\overline{y_d}$ relative overall uncertainty (1 SD) against measured events with two different lower detection thresholds. Dashed lines: spectrum without ^{10}B. Full lines: spectrum with 100 ppm of ^{10}B.

By remembering that $n(y_i)=n\cdot f(y_i)$ where $f(y_i)$ is the value of the probability density function at y_i and n is the sum of all the measured events and changing the lower sum limit in the denominator of the 3rd addendum (in such a way the 3rd addendum value will be bigger than that one it ought to be), the relative uncertainty can written as function of $f(y)$:

$$\left(\frac{\sigma_{\overline{y_d}}}{\overline{y_d}}\right)^2 < \left(\frac{\sigma_{F_{cal}}}{F_{cal}}\right)^2 + \frac{\left(0.5\cdot\sum_{0.01}^{y_{thr}} y_i^2\cdot f(y_i)^{extr}\Delta y_i\right)^2}{\left(\sum_{0.01}^{y_{max}} y_i^2\cdot f(y_i)\cdot\Delta y_i\right)^2} + \frac{\sum_{y_{thr}}^{y_{max}} y_i^4\cdot f(y_i)\cdot\Delta y_i}{n\cdot\left(\sum_{y_{thr}}^{y_{max}} y_i^2\cdot f(y_i)\cdot\Delta y_i\right)^2} + \frac{\sum_{y_{thr}}^{y_{max}} y_i^2\cdot f(y_i)\cdot\Delta y_i}{n\cdot\left(\sum_{y_{thr}}^{y_{max}} y_i\cdot f(y_i)\cdot\Delta y_i\right)^2} \tag{24}$$

Where the ratio $_{Fcal}/F_{cal}$ value is 0.048 when the lineal energy calibration is made with the electron edge of a pure photon field (see paragraph 4).

In figure 10, the $\overline{y_d}$ relative overall uncertainties of the two spectra of figure 2 are plotted against total events and for different lower detection thresholds. Figure 10 shows that the lower detection threshold affects very few the $\overline{y_d}$ value. Only at 0 ppm of ^{10}B and for more than 10^6 events changes in the lower detection threshold are significant. Event statistics plays a bigger role. For a lower detection threshold of 0.1 keV/μm and 10^7 events, the $\overline{y_d}$ overall uncertainty is 5.36%, when 0 ppm of ^{10}B is added, and 4.91%, when 100 ppm of ^{10}B is added. These values are close to the lineal calibration uncertainty. There is not significant advantage to have more the 10^7 events. On the contrary, less total events increase the $\overline{y_d}$ uncertainty.

9. Overall uncertainty of *RBE*

Remembering the ***RBE*** definition (equation 2) and the ***d(y)*** definition (equation 17), we obtain the ***RBE*** definition:

$$RBE = \frac{\sum_{0.01}^{y_{thr}} r(y_i)\cdot y_i\cdot n(y_i)\cdot\Delta y_i + \sum_{y_{thr}}^{y_{max}} r(y_i)\cdot y_i\cdot n(y_i)\cdot\Delta y_i}{\sum_{0.01}^{y_{max}} y_i\cdot n(y_i)\cdot\Delta y_i} \tag{25}$$

In equation 25 we can not changing everywhere the y-variable by using the equation $y_i = F_{cal}\cdot\tilde{y}_i$, since $r(y_i)$ is a literature function [13] given in keV/μm not in Volt. However, the weighting function $r(y_i)$ is 1 for y < 10 keV/μm (see figure 8). Since we can assume that the low threshold y_{thr} is always less than 10 keV/μm, we can simplify the equation 23 and obtaining:

$$RBE = \frac{\sum_{0.01}^{y_{thr}} y_i\cdot n(y_i)\cdot\Delta y_i + \sum_{y_{thr}}^{y_{max}} r(y_i)\cdot y_i\cdot n(y_i)\cdot\Delta y_i}{\sum_{0.01}^{y_{max}} y_i\cdot n(y_i)\cdot\Delta y_i} \tag{26}$$

Now we can substitute y with $\tilde{y}$, where that is possible:

$$RBE = \frac{F_{cal} \cdot \sum_{\tilde{y}\min}^{\tilde{y}_{thr}} \tilde{y}_i \cdot n(\tilde{y}_i) \cdot \Delta\tilde{y}_i + \sum_{y_{thr}}^{y_{\max}} r(y_i) \cdot y_i \cdot n(y_i) \cdot \Delta y_i}{F_{cal} \cdot \sum_{\tilde{y}\min}^{\tilde{y}_{\max}} \tilde{y}_i \cdot n(\tilde{y}_i) \cdot \Delta\tilde{y}_i} \tag{27}$$

From the error propagation formula, we obtain:

$$\left(\frac{\sigma_{RBE}}{RBE}\right)^2 = \left(\frac{\sigma_{num}}{num}\right)^2 + \left(\frac{\sigma_{den}}{den}\right)^2 \tag{28}$$

where ***num*** and ***den*** have the usual meaning. The numerator is made of two addenda:

$$\sigma_{num}^2 = \sigma_{extr}^2 + \sigma_{meas}^2 \tag{29}$$

Because the numerator first addendum (***extr***) is in its turn the product of two factors:

$$\sigma_{extr}^2 / extr^2 = \left(\frac{\sigma_{F_{cal}}^2}{F_{cal}^2} + \frac{\sigma_{extr(\tilde{y})}^2}{extr(\tilde{y})^2}\right) \tag{30}$$

where $extr(\tilde{y}) \equiv \sum_{\tilde{y}\min}^{\tilde{y}_{thr}} \tilde{y}_i \cdot n(\tilde{y}_i) \cdot \Delta\tilde{y}_i$ and $extr \equiv F_{cal} \cdot \sum_{\tilde{y}\min}^{\tilde{y}_{thr}} \tilde{y}_i \cdot n(\tilde{y}_i) \cdot \Delta\tilde{y}_i$. Substituting and applying the usual reasoning about systematic uncertainty to get $\sigma_{extr(\tilde{y})}$, we obtain:

$$\sigma_{extr}^2 = \left(\frac{\sigma_{F_{cal}}^2}{F_{cal}^2} + \frac{\left(0.5 \cdot \sum_{\tilde{y}\min}^{\tilde{y}_{thr}} \tilde{y}_i \cdot n(\tilde{y}_i) \cdot \Delta\tilde{y}_i\right)^2}{\left(\sum_{\tilde{y}\min}^{\tilde{y}_{thr}} \tilde{y}_i \cdot n(\tilde{y}_i) \cdot \Delta\tilde{y}_i\right)^2}\right) \cdot \left(F_{cal} \cdot \sum_{\tilde{y}\min}^{\tilde{y}_{thr}} \tilde{y}_i \cdot n(\tilde{y}_i) \cdot \Delta\tilde{y}_i\right)^2 \tag{31}$$

eventually, substituting $\tilde{y}_i = y_i / F_{cal}$ and remembering that $\tilde{y}_{\min}$ corresponds to 0.01 keV/µm:

$$\sigma_{extr}^2 = \left(\frac{\sigma_{F_{cal}}^2}{F_{cal}^2} + 0.25\right) \cdot \left(\sum_{0.01}^{y_{thr}} y_i \cdot n(y_i) \cdot \Delta y_i\right)^2 \equiv A \tag{32}$$

In the numerator of equation 27, the y-variable in the second addendum (***meas***) is in keV/µm, but it is not straightforward how taking into account the lineal calibration uncertainty for calculating this term overall uncertainty. The calibration uncertainty σ_{cal} changes the value of ***y·n(y)***, but not the value of ***r(y)***. Moreover, the changes in ***y·n(y)*** are due to the abscissa value uncertainty, which is independent on the event uncertainty. Therefore to assess σ^2_{meas} we first sum the relative squared error of $r(y_i)$ and $n(y_i)$ and then we add the absolute squared error due to calibration uncertainty. Remembering that ***n(y)*** is an event density:

$$\sigma^2_{meas} = \left(\frac{\sigma^2_{r(y)}}{r^2(y)} + \frac{\sigma^2_{\Delta y \cdot n(y)}}{\Delta y^2 \cdot n^2(y)} \right) \cdot meas^2 + \sigma^2_{cal} \tag{33}$$

To assess σ_{cal}, the multiplication in the second addendum (***meas***) is performed once with $n^+(y_i)$ and another time with $n^-(y_i)$. Where $n^+(y_i)$ is the event density obtained substituting y_i with $y_i+\sigma_i$ value and $n^-(y_i)$ the event density obtained substituting y_i with $y_i-\sigma_i$ value, being $\sigma_i=y_i \cdot \sigma_{Fcal}/F_{cal}$ the lineal energy standard deviation (see paragraph 4). The uncertainty σ_{cal} is then assumed to be half of the difference of the two products. This uncertainty is therefore half of the maximum error. This is true if the function ***n(y)*** in monotone, which is not true in general, but ***n(y)*** varies so smoothly that it can be assumed monotone inside the range $y_i-\sigma_F < y_i < y_i+\sigma_F$. Therefore:

$$\sigma^2_{meas} = \sum_{y_{thr}}^{y_{max}} \left(\frac{\sigma^2_{r(y_i)}}{r^2(y_i)} + \frac{1}{\Delta y_i \cdot n(y_i)} \right) \cdot r^2(y_i) \cdot y_i^2 \cdot n^2(y_i) \cdot \Delta y_i^2 + 0.25 \cdot r^2(y_i) \cdot y_i^2 \cdot \Delta y_i^2 \cdot \left[n^+(y_i) - n^-(y_i) \right]^2 \tag{34}$$

and simplifying

$$\sigma^2_{meas} = \sum_{y_{thr}}^{y_{max}} \left[\frac{\sigma^2_{r(y_i)}}{r^2(y_i)} \cdot n^2(y_i) + \frac{n(y_i)}{\Delta y_i} + 0.25 \cdot \left[n^+(y_i) - n^-(y_i) \right]^2 \right] \cdot r^2(y_i) \cdot y_i^2 \cdot \Delta y_i^2 \equiv B \tag{35}$$

The denominator of equation 27 is a normalisation factor, the uncertainty of which depends both on the $n(\tilde{y})$ statistics and on the calibration factor uncertainty. The calibration factor can be taken out of the sum, therefore, taking into account the observation used for the equation 12:

$$\left(\frac{\sigma_{den}}{den} \right)^2 < \frac{\sigma^2_{F_{cal}}}{F^2_{cal}} + \frac{\sum_{\tilde{y}_{th}}^{\tilde{y}_{max}} \tilde{y}_i^2 \cdot n(\tilde{y}_i) \cdot \Delta \tilde{y}_i}{\left(\sum_{\tilde{y}_{thr}}^{\tilde{y}_{max}} \tilde{y}_i \cdot n(\tilde{y}_i) \cdot \Delta \tilde{y}_i \right)^2} \tag{36}$$

Where we have substituted $\tilde{y}_{min}$ with $\tilde{y}_{thr}$ for preventing the "masking effect" due to extrapolated events. Since $y = F_{cal} \cdot \tilde{y}$, the relative denominator uncertainty is also:

$$\left(\frac{\sigma_{den}}{den} \right)^2 < \frac{\sigma^2_{F_{cal}}}{F^2_{cal}} + \frac{\sum_{y_{thr}}^{y_{max}} y_i^2 \cdot n(y_i) \cdot \Delta y_i}{\left(\sum_{y_{thr}}^{y_{max}} y_i \cdot n(y_i) \cdot \Delta y_i \right)^2} \tag{37}$$

Differently from $\overline{y_f}$ and $\overline{y_d}$ uncertainties, the ***RBE*** overall uncertainty cannot be completely separated in its three components; namely the lineal-energy calibration uncertainty, the systematic uncertainty due to the threshold and the event statistics uncertainty. By using the symbolic expressions ***A*** and ***B*** for the expressions 32 and 35, the equation 28 becomes :

$$\frac{\sigma^2_{RBE}}{RBE^2} < \frac{\sigma^2_{F_{cal}}}{F^2_{cal}} + \frac{A}{\left(\sum_{0.01}^{y_{max}} r(y_i)\cdot y_i \cdot n(y_i)\cdot \Delta y_i\right)^2} + \frac{B}{\left(\sum_{0.01}^{y_{max}} r(y_i)\cdot y_i \cdot n(y_i)\cdot \Delta y_i\right)^2} + \frac{\sum_{\tilde{y}_{thr}}^{y_{max}} y_i^2 \cdot n(y_i)\cdot \Delta y_i}{\left(\sum_{y_{thr}}^{y_{max}} y_i \cdot n(y_i)\cdot \Delta y_i\right)^2} \tag{38}$$

where the lineal-energy calibration uncertainty is presents both in ***A*** and on ***B***.

By remembering that $n(y_i)=n\cdot f(y_i)$ where $f(y_i)$ is the value of the probability density function at y_i and n is the sum of all the measured events, we can express the relative uncertainty as function of $f(y)$. Moreover, it is convenient to change the lower sum limit (from 0.01 to y_{thr}) in the denominator of the 3rd addendum of equation 38. With this change the denominator value decreases leading to overestimate the error. The expression 38 becomes:

$$\left(\frac{\sigma_{RBE}}{RBE}\right)^2 < \frac{\sigma^2_{F_{cal}}}{F^2_{cal}} + \frac{A}{\left(\sum_{y_{0.01}}^{y_{max}} r(y_i)\cdot y_i \cdot f(y_i)\cdot \Delta y_i\right)^2} + \frac{B}{n\cdot\left(\sum_{y_{thr}}^{y_{max}} r(y_i)\cdot y_i \cdot f(y_i)\cdot \Delta y_i\right)^2} + \frac{\sum_{\tilde{y}_{thr}}^{y_{max}} y_i^2 \cdot f(y_i)\cdot \Delta y_i}{n\cdot\left(\sum_{y_{thr}}^{y_{max}} y_i \cdot f(y_i)\cdot \Delta y_i\right)^2} \tag{39}$$

where ***A*** is:

$$A = \left(\frac{\sigma^2_{F_{cal}}}{F^2_{cal}} + 0.25\right)\cdot\left(\sum_{0.01}^{y_{thr}} y_i \cdot f(y_i)\cdot \Delta y_i\right)^2 \tag{40}$$

and ***B*** is:

$$B \equiv \sum_{y_{thr}}^{y_{max}} \left[\frac{\sigma^2_{r(y_i)}}{r^2(y_i)}\cdot n\cdot f^2(y_i) + \frac{f(y_i)}{\Delta y_i} + 0.25\cdot n\cdot\left[f^+(y_i) - f^-(y_i)\right]^2\right]\cdot r^2(y_i)\cdot y_i^2\cdot \Delta y_i^2 \tag{41}$$

being $f^+(y_i) = f(y_i+\sigma_i)$, $f^-(y_i) = f(y_i-\sigma_i)$ and $\sigma_i = y_i\cdot\sigma_{Fcal}/F_{cal}$.

However, considering $f(y)$ a straight line in the interval $y_i-\sigma_i<y_i<y_i+\sigma_i$, the squared of the difference $f^+(y_i)-f^-(y_i)$ can be approximated as:

$$[f^{+}(y_i) - f^{-}(y_i)]^2 \cong 4 \cdot [f(y_{i-1}) \cdot \frac{1 - \sigma_{F_{cal}} / F_{cal}}{1 - (y_i - y_{i-1})} - f(y_i)]^2 \qquad (41)$$

where y_i-y_{i-1} = ***0.96088***$\cdot y_i$ for 60 channel per decade. Therefore:

$$B \equiv \sum_{y_{thr}}^{y_{max}} \left[\frac{\sigma^2_{r(y_i)}}{r^2(y_i)} \cdot n \cdot f^2(y_i) + \frac{f(y_i)}{\Delta y_i} + n \cdot \left[f(y_{i-1}) \cdot \frac{1 - \sigma_{F_{cal}} / F_{cal}}{\mathbf{0.96088}} - f(y_i) \right]^2 \right] \cdot r^2(y_i) \cdot y_i^2 \cdot \Delta y_i^2 \qquad (42)$$

Now the dependency of ***B*** on the lineal calibration uncertainty is explicit.

The relative ***RBE*** uncertainty (inequality 39) is plotted in figure 11 for 0 ppm of ^{10}B and 100 ppm of ^{10}B. In both the cases, after 10^6 total events the ***RBE*** uncertainty reaches a plateau value, which depends on the lineal calibration uncertainty and on the detection lower threshold value. With the lower threshold value of 0.1 keV/µm and 10^6 measured events, the overall ***RBE*** uncertainty is **5.39%** and **6.24%** for 0 ppm of ^{10}B and 100 ppm of ^{10}B respectively.

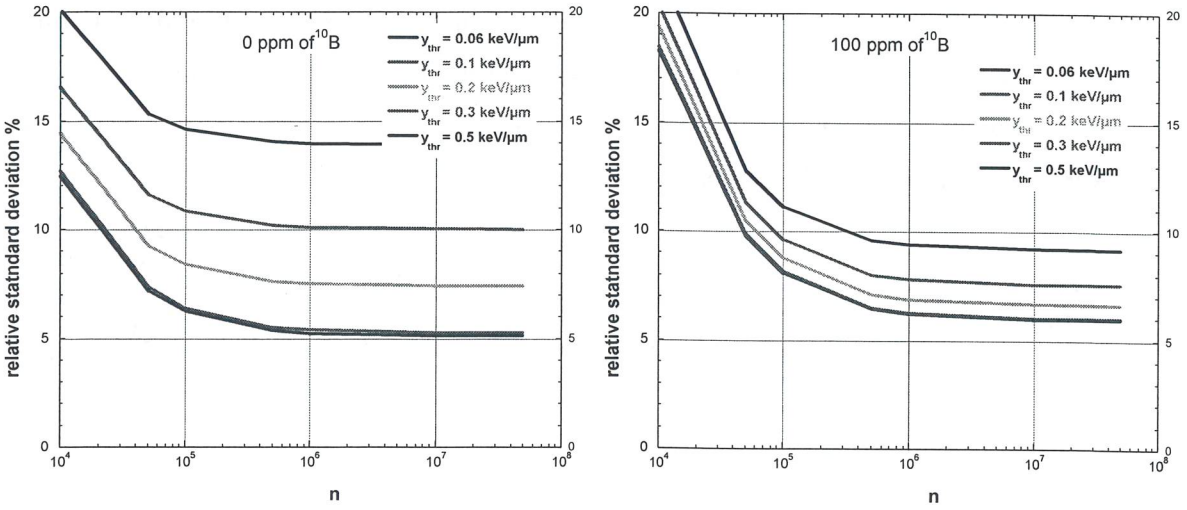

Figure 11. ***RBE*** relative overall uncertainty (1 SD) against measured events with different lower detection thresholds. Left side: spectrum without ^{10}B. Right side: spectrum with 100 ppm of ^{10}B. The weighting function used is plotted in figure 8.

10. Absorbed dose overall uncertainty

The dose ***D*** per reactor power monitor unit has been calculated with the following equation:

$$D = \frac{c \cdot \overline{y_f} \cdot n_{tot}}{Q} \qquad (43)$$

where $\overline{y_f}$ is the mean lineal energy calculated over all the mixed-field spectrum (extrapolated

down to 0.01 keV/μm); n_{tot} is the microdosimetric spectrum total event value (measured event value n plus the extrapolated event value):

$$n_{tot} = n \cdot \frac{\sum_{0.01}^{y_{max}} f(y_i) \cdot \Delta y_i}{\sum_{y_{thr}}^{y_{max}} f(y_i) \cdot \Delta y_i} \qquad (44)$$

where $\sum_{0.01}^{y_{max}} f(y_i) \cdot \Delta y_i = 1$

Q is the charge of the reactor power monitor and c is the calibration factor. In the following analysis we will disregard the c and Q uncertainties, which can be easily added in the experimental practice. Therefore, for sake of simplicity, we can re-write the absorbed dose per monitor unit and per calibration factor unit as:

$$D = \overline{y}_f \cdot n_{tot} \qquad (45)$$

and substituting n_{tot}:

$$D = n \cdot \frac{\sum_{0.01}^{y_{max}} f(y_i) \cdot \Delta y_i}{\sum_{y_{thr}}^{y_{max}} f(y_i) \cdot \Delta y_i} \cdot \sum_{0.01}^{y_{max}} y_i \cdot f(y_i) \cdot \Delta y_i \qquad (46)$$

Therefore the spectra of figure 2 (right side), which are normalised per unit of dose, can be re-plotted (figure 12) per monitor unit (we assume that the calibration factor is the same). In figure 12 the measured (not extrapolated) spectra are plotted; therefore n_{tot} has been substituted with n, since the extrapolated events are not included.

In figure 12, the "visual area" under the curve between y and $y+\Delta y$ is proportional to the dose, released per reactor monitor unit, due to events between y and $y+\Delta y$. 100 ppm of ^{10}B in the counter wall do not change significantly the gamma dose component (the higher gamma dose at low y-values for 0 ppm of ^{10}B is due a higher activation of the reactor, possibly), but increase showily the dose due to 300 KeV/μm events (BNC light ion events).

In order to calculate the D overall uncertainty, it is useful splitting equation 45 in two components, which we can conventionally call the dose D_{extr} due to extrapolated events and the gamma dose D_{meas} due to measured events:

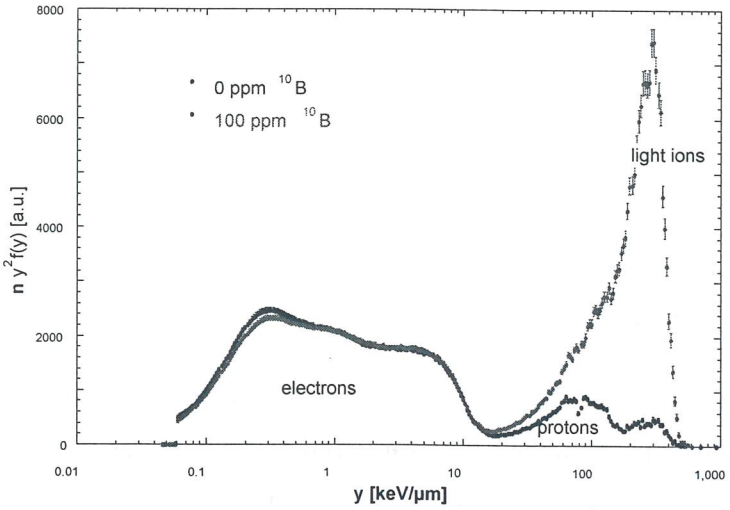

Figure 12. Microdosimetric spectra of figure 2 scaled for TEPC events per reactor monitor unit. The measured events ***n*** are different for the two spectra.

$$D = n_{tot} \cdot \overline{y}_f \Big|_{0.01}^{thr} + n_{tot} \cdot \overline{y}_f \Big|_{thr}^{\max} = D_{extr} + D_{meas} \tag{47}$$

The absorbed dose uncertainty is therefore:

$$\left(\frac{\sigma_D}{D}\right)^2 = \frac{\sigma^2_{D_{extr}}}{(D)^2} + \frac{\sigma^2_{D_{meas}}}{(D)^2} \tag{48}$$

The uncertainty of D_{extr} is highly dependent on the hypothesis about the shape of the under-threshold gamma events. Therefore, we consider D_{extr} as a systematic error (see paragraph 5):

$$\sigma_{D_{extr}} = \frac{1}{2} \cdot n_{tot} \cdot \sum_{0.01}^{y_{thr}} y_i \cdot f(y_i) \cdot \Delta y_i \tag{49}$$

$$\text{and} \quad \frac{\sigma^2_{D_{extr}}}{(D)^2} = 0.25 \cdot \frac{\left(\sum_{0.01}^{y_{thr}} y_i \cdot f(y_i) \cdot \Delta y_i\right)^2}{\left(\sum_{0.01}^{y_{\max}} y_i \cdot f(y_i) \cdot \Delta y_i\right)^2} \tag{50}$$

The D_{meas} relative uncertainty is:

$$\left(\frac{\sigma_{D_{meas}}}{D_{meas}}\right)^2 = \frac{1}{n_{tot}} + \left(\frac{\sigma\left(\overline{y}_f \Big|_{y_{thr}}^{y_{\max}}\right)}{\overline{y}_f \Big|_{y_{thr}}^{y_{\max}}}\right)^2 \tag{51}$$

therefore the D_{meas} uncertainty is:

$$\sigma^2_{D_{meas}} = n_{tot} \cdot \left(\overline{y_f} \Big|_{y_{thr}}^{y_{max}} \right)^2 + n_{tot}^2 \cdot \left[\sigma \left(\overline{y_f} \Big|_{y_{thr}}^{y_{max}} \right) \right]^2 \tag{52}$$

and

$$\left(\frac{\sigma_{D_{meas}}}{D} \right)^2 = \frac{\left(\overline{y_f} \Big|_{y_{thr}}^{y_{max}} \right)^2}{n_{tot} \cdot \left(\overline{y_f} \Big|_{0.01}^{y_{max}} \right)^2} + \left(\frac{\sigma \left(\overline{y_f} \Big|_{y_{thr}}^{y_{max}} \right)}{\overline{y_f} \Big|_{0.01}^{y_{max}}} \right)^2 \tag{53}$$

The $\overline{y_f}$ uncertainty has been already calculated (see equation 14 and inequality 15), therefore:

$$\left(\frac{\sigma_D}{D} \right)^2 = 0.25 \cdot \frac{\left(\sum_{0.01}^{y_{thr}} y_i \cdot f(y_i) \cdot \Delta y_i \right)^2}{\left(\sum_{0.01}^{y_{max}} y_i \cdot f(y_i) \cdot \Delta y_i \right)^2} + \frac{\left(\sum_{y_{thr}}^{y_{max}} y_i \cdot f(y_i) \cdot \Delta y \right)^2 + \sum_{y_{thr}}^{y_{max}} y^2{}_i \cdot f(y_i) \cdot \Delta y}{n \cdot \left(\sum_{0.01}^{y_{max}} y_i \cdot f(y_i) \cdot \Delta y_i \right)^2} + \left(\frac{\sigma_{F_{cal}}}{F_{cal}} \right)^2 +$$

$$+ \frac{1}{n \cdot \sum_{y_{thr}}^{y_{max}} f(y_i) \cdot \Delta y_i} \tag{54}$$

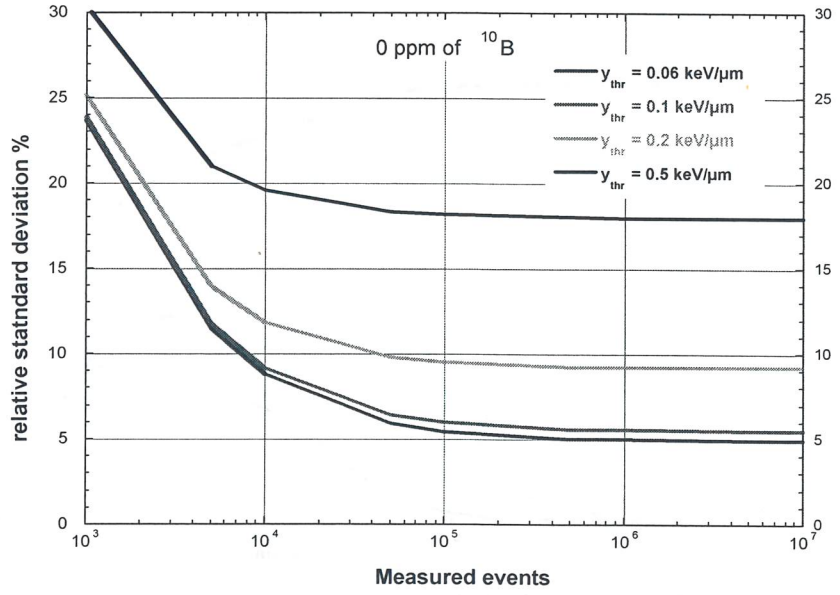

Figure 13. Total absorbed dose uncertainty against measured events for different low detection thresholds.

In figure 13, the 54-equation output is plotted for different n values and y_{thr}-values. For measured events more 10^5, the relative uncertainty reaches a constant value, which depends on the y_{thr}-value. For y_{thr}-values bigger that 0.2 keV/μm a high accuracy of the energy calibration is useless.

11. Gamma dose-component overall uncertainty

Microdosimetric spectra have been used to calculate dose components of the mixed radiation field [4]. Following equation 45, the gamma dose of the mixed field in TAPIRO reactor is the number of gamma events multiplied by the gamma event mean size:

$$D^{\gamma} = n_{tot} \cdot F_1 \cdot \overline{y_f}^{\gamma} \tag{55}$$

where $\overline{y_f}^{\gamma}$ is the frequency-weighted mean y-value of gamma events (comprehending the extrapolated events) and F_1 is the fraction of mixed-field event number due to gamma rays ($F_1 < 1$).

For calculating D^{γ}, we have first constructed a virtual γ-spectrum made of the measured y-spectrum plus the electron edge, which is known to be invariant with the gamma energy. In order to decide where adding the invariant electron edge, the gamma spectra of figure 6 have been re-plotted after being properly scaled in order to superimpose their electron edges (see figure 14). In figure 13 is also plotted the relative standard deviation (SD) of the four $y^2n(y)$ values.

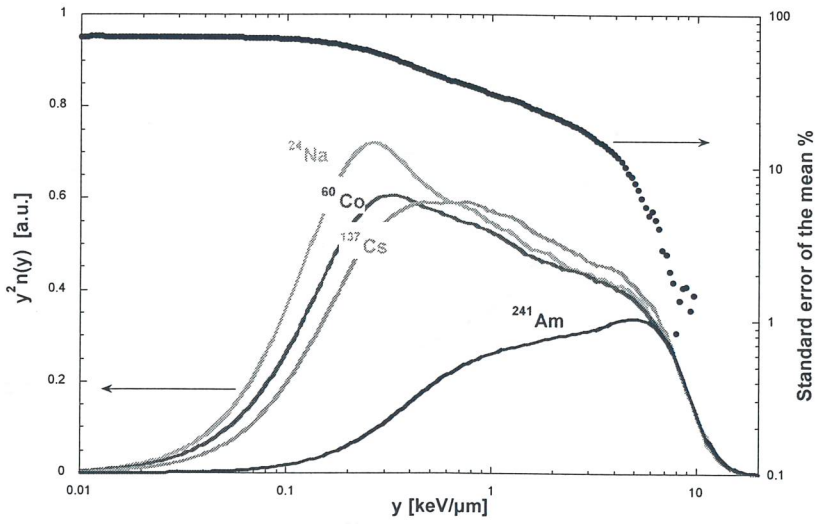

Figure 14. Microdosimetric spectra of figure 6 properly scaled in order to superimpose their electron edges. The full dots are the relative standard deviation of the 4 spectra $y^2n(y)$ values (see text).

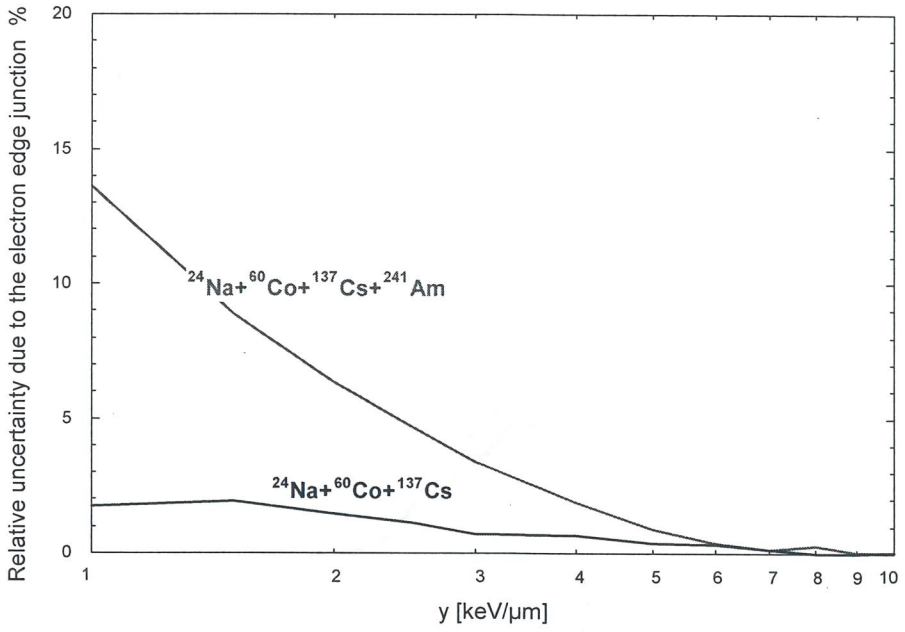

Figure 15. Relative standard deviation of $\overline{y_f}^{\gamma}$ value due to the electron-edge junction uncertainty (see figure 14) against the y-value of the junction. Red line: SD when all the four gamma spectra are taken into account. Blue line: SD when only three gamma spectra are taken into account (see text).

The average SD is 5.4% for y-values between 5 keV/μm and 7 keV/μm. It is about 1% for y-values bigger than 7 keV/μm whilst it increase steeply at y-values lower than 5 keV/μm. For any microdosimetric spectrum, we have therefore generated a "virtual-gamma" spectrum by adding to the low-y part the invariant electron edge.

However, it is not always possible to attach the electron edge in the region where it is really invariant, namely for y > 7keV/μm. In fact, this procedure assumes that the ion contribution to y-events is negligible for y-values less than electron-edge junction. It is therefore worthwhile re-defining the electron-edge as the microdosimetric spectrum averaged on all the microdosimetric spectra due to all the gamma energies and calculating the $y^2n(y)$ value dispersion around the mean after having superimposed the real electron edges as in figure 14. Because of this value dispersion, the $y^2n(y)$ value at which to attach the invariant part of the gamma spectrum has an error. In order to calculate the influence of such an uncertainty on $\overline{y_f}^{\gamma}$, we have multiplied it by the relative weight of the added gamma component in determining the $\overline{y_f}^{\gamma}$ value. This last uncertainty is plotted in figure 15 against the y-value at which the common part is attached. When all the four gamma sources are used (ranging about 2.6 MeV down to 60 keV) the

common part has to be added at $y > 5$ keV/µm to obtain less than 1% of uncertainty. If low-energy gamma rays can be excluded, the y-value limit at which the junction uncertainty weight less than 1% on the $\overline{y_f}^{\gamma}$ value uncertainty becomes 2.5 keV/µm (see figure 15).

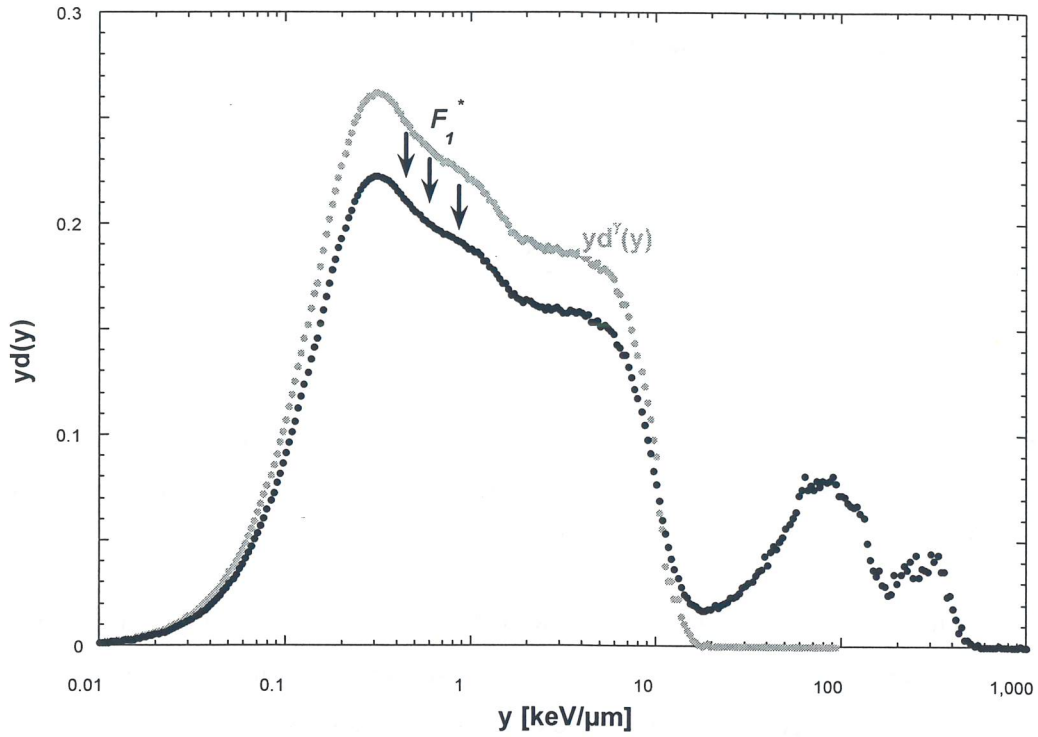

Figure 16. Microdosimetric spectra with 0 ppm of ^{10}B and "virtual-gamma" ***yd (y)*** spectrum (see text). The virtual-gamma spectrum is scaled down of a factor F_1^* to superimpose the mixed-field microdosimetric spectrum for y-values smaller than the electron-edge junction y-value (see text).

After having re-normalised the virtual-gamma spectrum to obtain $f^{\gamma}(y)$ the $\overline{y_f}^{\gamma}$ value is calculated. $f^{\gamma}(y)$ is then scaled down of a factor F_1 to match the mixed-field spectrum $f(y)$ in the region less than 5 keV/µm. $f^{\gamma}(y)$ and $f(y)$ differ of less than 0.1%; therefore the difference is hardly visible. More visible is the difference between the dose-weighted spectra $yd^{\gamma}(y)$ and $yd(y)$ (see figure 16), because the scaling factor F_1^* is smaller than F_1:

$$F_1^* = F_1 \cdot \frac{\overline{y_f^{\gamma}}}{\overline{y_f}} \tag{56}$$

Following equation 46, D^{γ} is therefore:

$$D^{\gamma} = n \cdot \frac{\sum_{0.01}^{y_{max}} f(y_i) \cdot \Delta y_i}{\sum_{y_{thr}}^{y_{max}} f(y_i) \cdot \Delta y_i} \cdot F_1 \cdot \sum_{0.01}^{y_{max}} y_i \cdot f^{\gamma}(y_i) \cdot \Delta y_i \qquad (57)$$

In order to calculate the D^{γ} overall uncertainty, it is useful splitting equation 57 in two components, as well as done for the D uncertainty calculation.

We can conventionally call D^{γ}_{extr} the gamma dose due to extrapolated events and D^{γ}_{meas} the gamma dose due to measured events:

$$D^{\gamma} = n_{tot} \cdot F_1 \cdot \overline{y_f}^{\gamma}\Big|_{0.01}^{thr} + n_{tot} \cdot F_1 \cdot \overline{y_f}^{\gamma}\Big|_{thr}^{max} = D^{\gamma}_{extr} + D^{\gamma}_{meas} \qquad (58)$$

The gamma dose uncertainty is therefore:

$$\left(\frac{\sigma_{D^{\gamma}}}{D^{\gamma}}\right)^2 = \frac{\sigma^2_{D^{\gamma}_{extr}}}{\left(D^{\gamma}\right)^2} + \frac{\sigma^2_{D^{\gamma}_{meas}}}{\left(D^{\gamma}\right)^2} + \frac{\sigma^2_{D^{\gamma}_{junc}}}{\left(D^{\gamma}\right)^2} \qquad (59)$$

where $\sigma^2_{D^{\gamma}_{junc}}$ is the uncertainty of the dose due to the uncertainty of the electron edge junction.

The electron-edge junction relative uncertainty produce an uncertainty on $\overline{y_f}^{\gamma}$. We have constructed a virtual-gamma spectra with an average electron-edge in the 5-7 keV/μm region, the uncertainty of which is 5.4% (see figure 13). This uncertainty regards less than 15% of the contribution to $\overline{y_f}^{\gamma}$. Therefore, with our choice, it contributes for less than 0.81% to overall $\overline{y_f}^{\gamma}$ uncertainty:

$$\frac{\sigma^2_{D^{\gamma}_{junc}}}{\left(D^{\gamma}\right)^2} = 0.0081^2 \qquad (60)$$

The scaling factor F_1 disappears in error formulas, because it is assumed to have not error. The superimposition is in fact performed in the region (y ≤ 5 keV/μm) where virtual-gamma spectrum and mixed-field spectrum are the same. The gamma dose-component uncertainty can be therefore calculated with the equation 54, where $f^{\gamma}(y)$ substitutes $f(y)$ the gamma event number n_{γ} substitutes n_{tot}. However, in the spectra of figure 2, $n_{\gamma} = 0.9990 \cdot n_{tot}$ and $n_{\gamma} = 0.9975 \cdot n_{tot}$ for 0 ppm and 100 ppm of ^{10}B respectively. Therefore the substitution, for sake of simplicity, of n_{γ} with n does not really change the overall uncertainty assessment. Finally we obtain:

$$\left(\frac{\sigma^{\gamma}{}_{D}}{D^{\gamma}}\right)^2 = 0.25 \cdot \frac{\left(\sum_{0.01}^{y_{thr}} y_i \cdot f^{\gamma}(y_i) \cdot \Delta y_i\right)^2}{\left(\sum_{0.01}^{y_{max}} y_i \cdot f^{\gamma}(y_i) \cdot \Delta y_i\right)^2} + \frac{\left(\sum_{y_{thr}}^{y_{max}} y_i \cdot f^{\gamma}(y_i) \cdot \Delta y\right)^2 + \sum_{y_{thr}}^{y_{max}} y_i^2 \cdot f^{\gamma}(y_i) \cdot \Delta y}{n \cdot \left(\sum_{0.01}^{y_{max}} y_i \cdot f^{\gamma}(y_i) \cdot \Delta y_i\right)^2} + \left(\frac{\sigma_{F_{cal}}}{F_{cal}}\right)^2 +$$

$$+ \frac{1}{n \cdot \sum_{y_{thr}}^{y_{max}} f^{\gamma}(y_i) \cdot \Delta y_i} + 0.0081^2 \qquad (61)$$

The gamma dose component of the 100 ppm ^{10}B spectrum is slightly different, because of the presence of 0.48 MeV gamma rays of the emerging from the ^{11}B fission and because the measurement was performed in an other time with different gamma background. The gamma-dose component can be calculated with the expression 55, where the factor F_1 is substituted with the factor F_2, which is the fraction of 100 ppm ^{10}B spectrum events due to gamma rays.

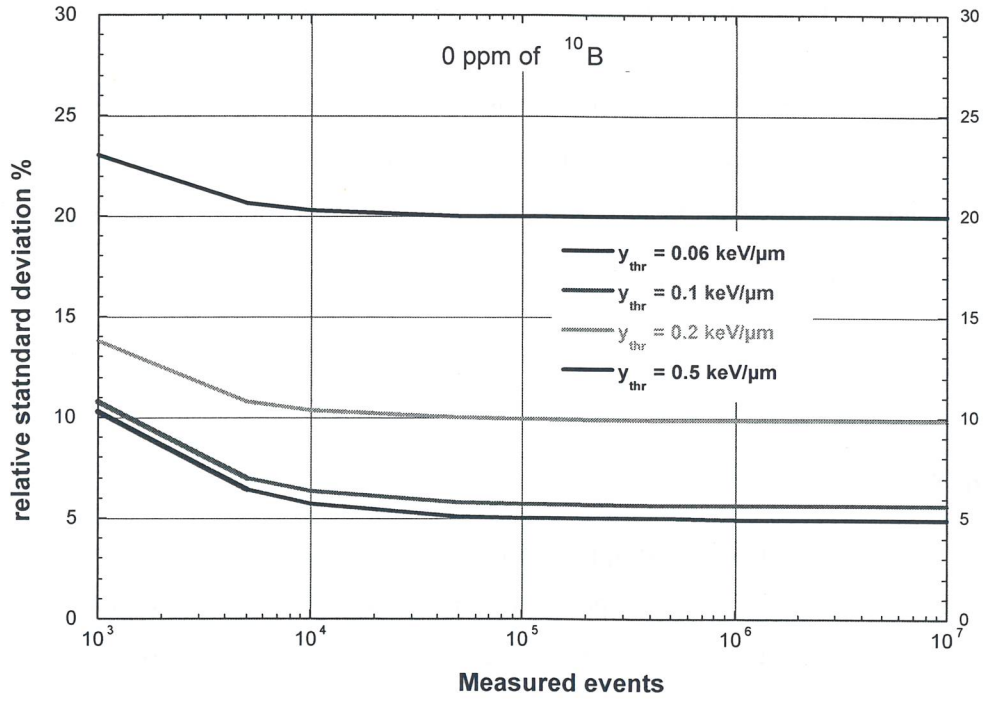

Figure 17. Gamma dose-component uncertainty against measured events for different low detection thresholds.

In figure 17, the 61-equation output is plotted for different n values (measured events) and y_{thr}-values. The gamma dose-component uncertainty is almost independent on the event statistics for more than 10^4 events. It depends strongly on the y_{thr}-value Note that with high measurement

thresholds (y_{thr}-value > 0.2 keV/µm) a high energy-calibration accuracy is useless, as for the total dose (see figure 13).

12. Neutron dose-component overall uncertainty

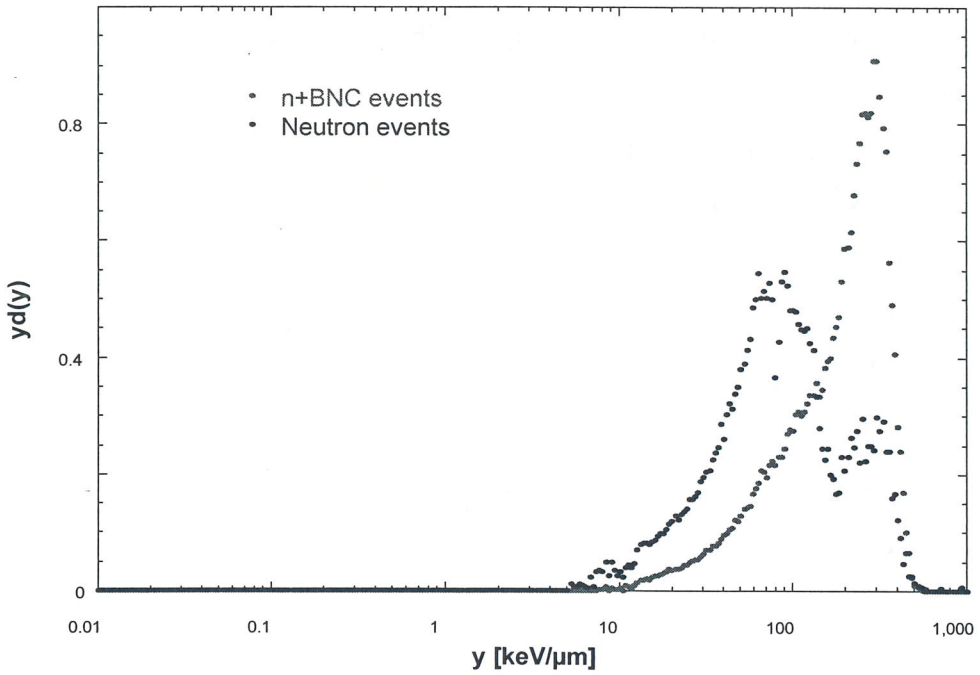

Figure 18. Microdosimetric spectra of n+BNC events and of neutron events on the tissue-equivalent TEPC plastic. The spectra have been obtained subtracting the gamma-due events from 100 ppm and 0 ppm of ^{10}B microdosimetric spectra (see text). Spectra are normalised to n+BNC dose unity and to neutron dose unity, respectively.

After the virtual-gamma spectrum subtraction, the density probability of the neutron-due events $f^n(y)$ is calculated for 0 ppm of ^{10}B. It is used to calculate the neutron-due mean event size $\overline{y}_f^n$. Similarly, the density probability of the neutron-due events for 100 ppm of ^{10}B $f^{n+BNC}(y_i)$ can be calculated together with the neutron-due mean event size $\overline{y}_f^{n+BNC}$. The superscript ***n+BNC*** points out that the events are due both to ordinary neutron reaction on the tissue-equivalent plastic and to the fragments of the Boron neutron-capture reactions. The dose-weighted microdosimetric spectra of neutron events and ***n+BNC*** events are plotted in figure 18.

The neutron dose can be calculated with the following algorithm:

$$D^n = n_{tot} \cdot (1 - F_1) \cdot \overline{y_f}^n \tag{62}$$

and then:

$$D^n = n \cdot \frac{\sum_{0.01}^{y_{max}} f(y_i) \cdot \Delta y_i}{\sum_{y_{thr}}^{y_{max}} f(y_i) \cdot \Delta y_i} \cdot (1 - F_1) \cdot \sum_{0.01}^{y_{max}} y_i \cdot f^n(y_i) \cdot \Delta y_i \tag{63}$$

where $f^n(y_i)$ is the probability density distribution of the difference mixed-field events minus gamma events:

$$f^n(y_i) = \frac{f(y_i) - F_1 \cdot f^\gamma(y_i)}{\sum_{0.01}^{y_{max}} [f(y_i) - F_1 \cdot f^\gamma(y_i)] \cdot \Delta y_i} \tag{64}$$

therefore:

$$D^n = n \cdot \frac{\sum_{0.01}^{y_{max}} f(y_i) \cdot \Delta y_i}{\sum_{y_{thr}}^{y_{max}} f(y_i) \cdot \Delta y_i} \cdot (1 - F_1) \cdot \frac{\sum_{0.01}^{y_{max}} y_i \cdot f(y_i) \cdot \Delta y_i - F_1 \cdot \sum_{0.01}^{y_{max}} y_i \cdot f^\gamma(y_i) \cdot \Delta y_i}{\sum_{0.01}^{y_{max}} [f(y_i) - F_1 \cdot f^\gamma(y_i)] \cdot \Delta y_i} \tag{65}$$

Since $1\text{-}F_1$ has not error:

$$\left(\frac{\sigma_{D^n}}{D^n}\right)^2 = \left(\frac{\sigma_{n_{tot}}}{n_{tot}}\right)^2 + \left(\frac{\sigma_{\overline{y_f}^n}}{\overline{y_f}^n}\right)^2 \tag{66}$$

Remembering that the under-threshold y-events do not contribute to D^n as well as to $\overline{y_f}^n$, we obtain:

$$\left(\frac{\sigma_{D^n}}{D^n}\right)^2 = \frac{1}{n} + \left(\frac{\sigma_{F_{cal}}}{F_{cal}}\right)^2 + \frac{\sum_{y_{thr}}^{y_{max}} y_i^2 \cdot f^n(y_i) \cdot \Delta y_i}{n_n \cdot \left(\sum_{y_{thr}}^{y_{max}} y_i \cdot f^n(y_i) \cdot \Delta y_i\right)^2} + \frac{1}{n_n \cdot \sum_{y_{thr}}^{y_{max}} f^n(y_i) \cdot \Delta y_i} \tag{67}$$

where n_n is the neutron-due event number. For "neutron-due event number" we intend only the events due to ions set in motion by the neutron reactions. Events due to prompt gamma rays and delayed gamma rays are computed in the gamma dose component D^γ; therefore:

$$n_n = n_{tot} \cdot \sum_{0.01}^{y_{max}} \left[f(y_i - F_1 \cdot f^\gamma(y_i) \right] \cdot \Delta y_i \tag{68}$$

and of course:

$$n_n \cdot f^n(y_i) = n_{tot} \cdot \left[f(y_i - F_1 \cdot f^\gamma(y_i) \right] \tag{69}$$

Therefore:

$$\left(\frac{\sigma_{D^n}}{D^n}\right)^2 = \frac{1}{n} + \left(\frac{\sigma_{F_{cal}}}{F_{cal}}\right)^2 + \frac{\sum_{y_{thr}}^{y_{max}} y_i^2 \cdot f(y_i) \cdot \Delta y_i - F_1 \cdot \sum_{y_{thr}}^{y_{max}} y_i^2 \cdot f^\gamma(y_i) \cdot \Delta y_i}{n_{tot} \cdot \left(\sum_{y_{thr}}^{y_{max}} y_i \cdot f(y_i) \cdot \Delta y_i - F_1 \cdot \sum_{y_{thr}}^{y_{max}} y_i \cdot f^\gamma(y_i) \cdot \Delta y_i \right)^2} +$$

$$+ \frac{1}{n_{tot} \cdot \left(\sum_{y_{thr}}^{y_{max}} f(y_i) \cdot \Delta y_i - F_1 \cdot \sum_{y_{thr}}^{y_{max}} f^\gamma(y_i) \cdot \Delta y_i \right)} \tag{70}$$

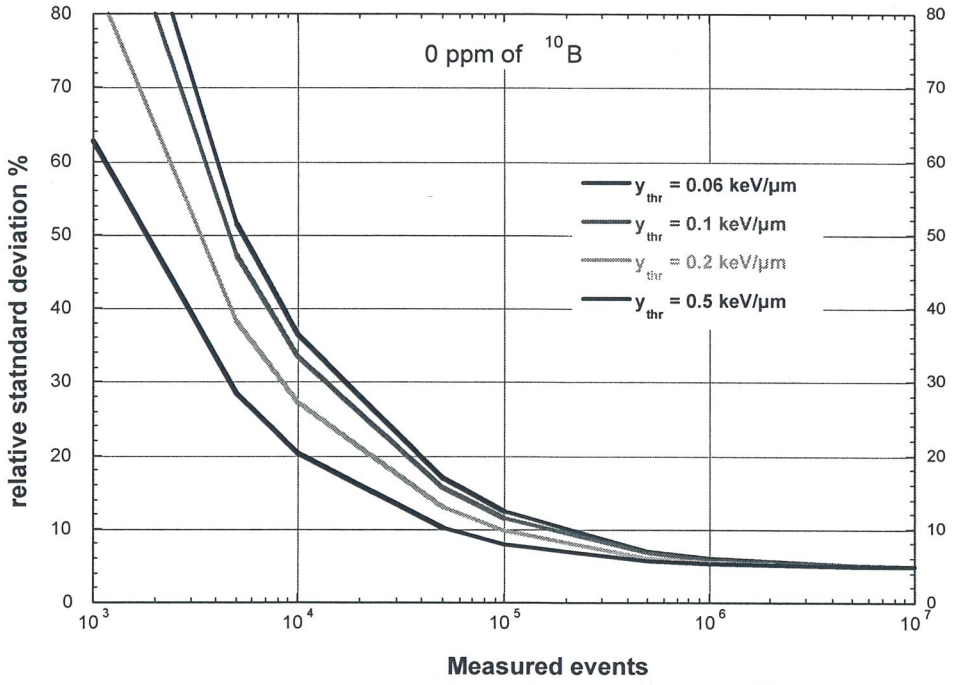

Figure 19. Neutron dose-component uncertainty against measured events for different low detection thresholds.

In figure 19, the 70-equation output is plotted for different n values (measured events) and y_{thr}-values. For measured events more 10^6, the relative uncertainty is almost independent on the y_{thr}-value and it approaches the energy calibration uncertainty, which, in our case is 4.8%. $\frac{\sigma_{D^n}}{D^n}$ behaviour affects the $\frac{\sigma_D}{D}$ behaviour only for measured events less than 10^5 (see figure 13).

When a TEPC with borated cathode is used, we have a neutron dose plus a BNC dose. After the gamma subtraction, we obtain:

$$D^{n+BNC} = n_{tot} \cdot (1 - F_2) \cdot \overline{y}_f^{\,n+BNC} \tag{71}$$

It can calculated with the equation 65 where F_2 substitutes F_1. Since all the events are bigger than the y_{thr}-value, the overall uncertainty can be written, similarly to the equation 67:

$$\left(\frac{\sigma_{D^{n+BNC}}}{D^{n+BNC}}\right)^2 = \frac{1}{n_{tot}} + \left(\frac{\sigma_{F_{cal}}}{F_{cal}}\right)^2 + \frac{\sum_{y_{thr}}^{y_{max}} y_i^{\,2} \cdot f^{n+BNC}(y_i) \cdot \Delta y_i}{n_{n+BNC} \cdot \left(\sum_{y_{thr}}^{y_{max}} y_i \cdot f^{n+BNC}(y_i) \cdot \Delta y_i\right)^2} + \frac{1}{n_{n+BNC} \cdot \sum_{y_{thr}}^{y_{max}} f^{n+BNC}(y_i) \cdot \Delta y_i} \tag{72}$$

where n_{n+BNC} is the neutron-due event number. For "neutron-due event number" we intend here only the events due to ions set in motion by the neutron reactions, ^{11}B fission fragments included. Events due to prompt gamma rays and delayed gamma rays are computed in the gamma dose component D^{γ}. Therefore:

$$n_{n+BNC} = n_{tot} \cdot \sum_{0.01}^{y_{max}} \left[f(y_i - F_2 \cdot f^{\gamma}(y_i) \right] \cdot \Delta y_i \tag{73}$$

and

$$f^{n+BNC}(y_i) = \frac{f(y_i) - F_2 \cdot f^{\gamma}(y_i)}{\sum_{0.01}^{y_{max}} [f(y_i) - F_2 \cdot f^{\gamma}(y_i)] \cdot \Delta y_i} \tag{74}$$

Therefore D^{BNC} relative uncertainty can be calculated with the equations 70, just substituting F_1 with F_2.

13. BNC dose-component overall uncertainty

The BNC dose-component could be simply calculated as:

$$D^{BNC} = D^{n+BNC} - D^{n} = n_{tot} \cdot (1 - F_2) \cdot \overline{y}_f^{\,n+BNC} - n_{tot} \cdot (1 - F_1) \cdot \overline{y}_f^{\,n} \tag{75}$$

however this procedure is not very precise, because we must sum the $\overline{y}_f^{\,n+BNC}$ uncertainty and the $\overline{y}_f^{\,n}$ uncertainty.

A more precise procedure consists in multiplying the frequency spectrum with 0 ppm of ^{10}B, $f_0(y)$, by the measured event number n_0 and subtracting the result from the frequency spectrum

with 100 ppm of ^{10}B, $f_{100}(y)$, multiplied by the measured event number n_{100}. Note that, this procedure doesn't need process extrapolated microdosimetric spectra; therefore we do not have the related uncertainty. The dose-weighted distributions of these two not-normalised spectra are plotted in figure 12. The BNC-due events $n^{BNC}(y_i)$ are then:

$$n^{BNC}(y_i) = \left| n_{100} \cdot f_{100}(y_i) - n_0 \cdot f_0(y_i) \right|_{10}^{y_{max}} \tag{76}$$

where the symbol $\left|_{10}^{y_{max}}\right.$ means that only the events of y > 10 keV/μm are taken into account. For y < 10 keV/μm, the small differences in the two gamma fields give rise to both positive and negative events, which are not correlated with the BNC dose. The BNC dose is then:

$$D^{BNC} = n_{BNC} \cdot \overline{y_f^{BNC}} \tag{77}$$

where:

$$n_{BNC} = \sum_{10}^{y_{max}} \left[n_{100} \cdot f_{100}(y_i) - n_0 \cdot f_0(y_i) \right] \cdot \Delta y_i \tag{78}$$

and

$$\overline{y_f^{BNC}} = \sum_{10}^{y_{ma}} y_i \cdot f^{BNC}(y_i) \cdot \Delta y_i \tag{79}$$

where $f^{BNC}(y)$ is the probability density function of the $n^{BNC}(y_i)$ events (only the α and ^7Li events, whilst gamma events are taken into accounts in D^{γ}).

$$f^{BNC}(y_i) = \frac{\left| n_{100} \cdot f_{100}(y_i) - n_0 \cdot f_0(y_i) \right|_{10}^{y_{max}}}{\sum_{10}^{y_{max}} \left[n_{100} \cdot f_{100}(y_i) - n_0 \cdot f_0(y_i) \right] \cdot \Delta y_i} \tag{80}$$

The dose-weighted distribution of $n^{BNC}(y_i)$ events is plotted in figure 17 together with the neutron-due event (without BNC events) distribution.

Sine the n_{BNC} value and the normalisation factor of equation 76 elide:

$$D^{BNC} = \sum_{10}^{y_{max}} \left| n_{100} \cdot f_{100}(y_i) - n_0 \cdot f_0(y_i) \right|_{10}^{y_{max}} \cdot y_i \cdot \Delta y_i \tag{81}$$

From the equation 77, the BNC dose uncertainty is:

$$\left(\frac{\sigma^{BNC}}{D^{BNC}} \right)^2 = \frac{1}{n_{BNC}} + \left(\frac{\sigma_{F_{cal}}}{F_{cal}} \right)^2 + \frac{\sum_{10}^{y_{max}} y_i^2 \cdot f^{BNC}(y_i) \cdot \Delta y_i}{n_{BNC} \cdot \left(\sum_{10}^{y_{max}} y_i \cdot f^{BNC}(y_i) \cdot \Delta y_i \right)^2} + \frac{1}{n_{BNC} \cdot \sum_{10}^{y_{max}} f^{BNC}(y_i) \cdot \Delta y_i} \tag{82}$$

and substituting n_{BNC} and $f^{BNC}(y_i)$ we obtain:

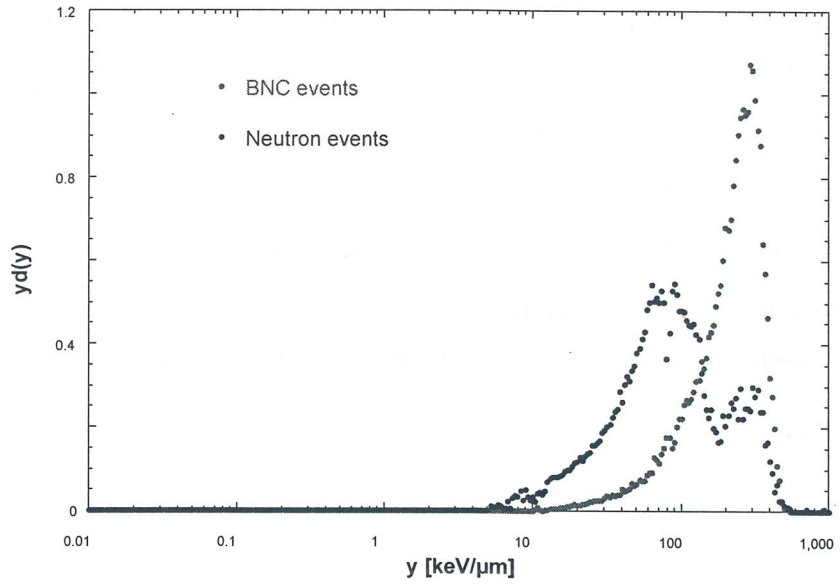

Figure 20. Microdosimetric spectra of BNC events and of neutron events on the tissue-equivalent TEPC plastic without ^{10}B. The BNC event spectrum has been obtained subtracting the frequency spectra of figure 12 and re-normalising the difference events (see text). Spectra are normalised to BNC dose unity and to neutron dose unity, respectively.

$$\left(\frac{\sigma^{BNC}}{D^{BNC}}\right)^2 = \frac{1}{\sum_{10}^{y_{max}}\left[n_{100}\cdot f_{100}(y_i) - n_0\cdot f_0(y_i)\right]\cdot \Delta y_i} + \frac{\sum_{10}^{y_{max}} y_i^{\,2}\cdot\left|n_{100}\cdot f_{100}(y_i) - n_0\cdot f_0(y_i)\right|_{10}^{y_{max}}\cdot \Delta y_i}{\left(\sum_{10}^{y_{max}} y_i\cdot\left|n_{100}\cdot f_{100}(y_i) - n_0\cdot f_0(y_i)\right|_{10}^{y_{max}}\right)\cdot \Delta y_i}^2 +$$

$$+\frac{1}{\sum_{10}^{y_{max}}\left|n_{100}\cdot f_{100}(y_i) - n_0\cdot f_0(y_i)\right|_{10}^{y_{max}}\cdot \Delta y_i} + \left(\frac{\sigma_{F_{cal}}}{F_{cal}}\right)^2 \qquad (83)$$

In figure 21, the 83-equation output is plotted for different n values and y_{thr}-values. For measured events more 10^6, the relative uncertainty is almost independent on the y_{thr}-value and it approaches the energy calibration uncertainty, which, in our case is 4.8%. The $\frac{\sigma_{D^{BNC}}}{D^{BNC}}$ behaviour is very close to the $\frac{\sigma_{D^n}}{D^n}$ behaviour (see figure 19), because it depends only on the large y-values. Although $\frac{\sigma_{D^{BNC}}}{D^{BNC}}$ does not depend directly on the y_{thr}-value, it depends indirectly on it. In fact, a larger y_{thr}-value, for a given n value, means more high y-value events.

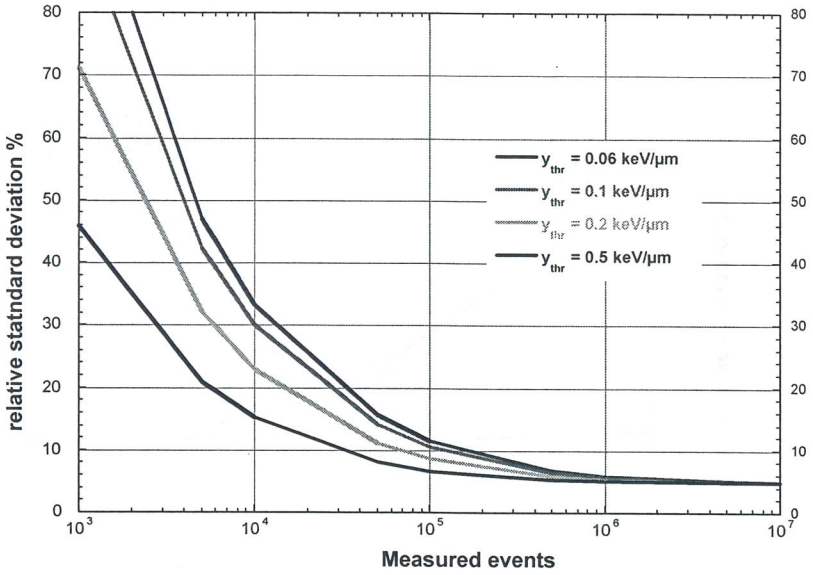

Figure 21. BNC dose-component uncertainty against measured events for different low detection thresholds.

14. Conclusions

We have calculated the overall uncertainties of the TEPC-measured dosimetric quantities of interest in the Boron neutron capture therapy. The relative standard deviations of gamma, neutron and BNC dose-components are plotted in figure 22 against the measured events and for a detection low threshold of 0.1 keV/µm.

This error analysis points out that it is necessary to have a low detection threshold of about 0.1 keV/µm and 10^6 measured events to obtain a relative uncertainty of about 5% for all the dose components (see figure 22).

If we apply the error analysis to the spectra of figure 2, the event statistics of which is $4.4 \cdot 10^7$ and $3.0 \cdot 10^7$ for 0 ppm and 100 ppm of ^{10}B respectively, we obtain the data of table 1. All the algorithms have been applied on the spectra extrapolated own to 0.01 keV/µm.

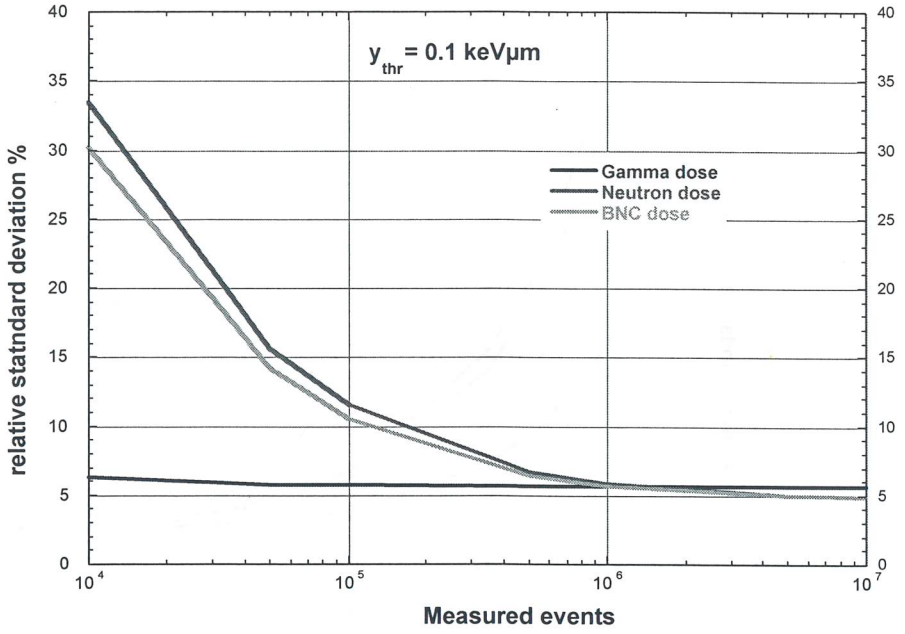

Figure 22. Comparison of the dose-component uncertainties against measured events for a low detection threshold of 0.1 keV/μm.

The relative overall uncertainties of the total dose, gamma dose and neutron dose of the spectrum with 0 ppm of ^{10}B and moreover the BNC dose, when 100 ppm of ^{10}B are present, are in table 2.

Table 1

Mean microdosimetric values of the spectra pf figure 2.

	$\overline{y_f}$	$\frac{\sigma_{\overline{y_f}}}{\overline{y_f}}$ %	$\overline{y_d}$	$\frac{\sigma_{\overline{y_d}}}{\overline{y_d}}$ %	RBE	$\frac{\sigma_{RBE}}{RBE}$ %
0 ppm ^{10}B	0.364 ± 0.014	**4.8**	18.70 ± 0.72	**4.97**	1.32 ± 0.05	**5.3**
100 ppm ^{10}B	0.614 ± 0.023	**4.8**	96.14 ± 3.53	**4.85**	1.44 ± 0.062	**5.7**

Table 2

Relative overall uncertainties of the doses measured with the spectra of figure 2.

	$\frac{\sigma_D}{D}$ %	$\frac{\sigma_{D^\gamma}}{D^\gamma}$ %	$\frac{\sigma_{D^n}}{D^n}$ %	$\frac{\sigma_{D^{BNC}}}{D^{BNC}}$ %
0 ppm ^{10}B	**4.8**	**4.9**	**4.8**	
100 ppm ^{10}B				**4.85**

References

[1] International Commision on Radiation Units and Measurements(ICRU) Report 36, *Microdosimetry*, 1983

[2] Waker AJ. Principles of experimental microdosimetry. Rad.Prot.Dosim. 61(4), 297-308, 1995.

[3] Pihet, P. Menzel, HG. Schmidt, R. Beauduin, M. Wambersie, A.*Biological weighting function for RBE specification of neutron therapy beams. Intercomparison of 9 European centres.* Rad. Prot Dosim. 31, 1990, pag.437-442.

[4] De Nardo, L. Seravalli, E. Rosi, G, Esposito, J. Colautti, P. Conte, V. Tornielli G. *BNCT microdosimetry at the TAPIRO reactor thermal column.* Rad.Prot.Dosim. 110, 579-586, 2004.

[5] Moro, D. Seravalli, E. Colautti, P. *Statistical and overall uncertainties in proton therapy microdosimetric measurements.* INFN-LNL Report 200/2003.

[6] Waker, AJ, *Experimental uncertainties in microdosimetric measurements*. Nucl.Ins. and Meth. A234, 354-360, 1985.

[7] Pihet, P. Gerdung, S. Grillmeyer RE. Kunz, A. Menzel, HG. *Critical assessment of calibration techniques for low pressure proportional counters in radiation dosimetry.* Rad.Prot.Dosim. 44, 115-120, 1992.

[8] Cesari, V. Colautti, P. Magrin, G. De Nardo, L. Baek, WJ. Grosswendt, B. Alkaa, A. Khamphan, C. Segur, P. Tornielli G. *Nanodosimetric measurements with an avalanche confinement TEPC.* Rad.Prot.Dosim. 99, 337-342, 2002.

[9] International Commission on Radiation Units and Measurements. Stopping powers and ranges for protons and alpha particles. Report 49. Bethesda, MD. ICRU Publications (1993).

[10] Comitè International des Poids et Mesures, Procès-Verbaux 49, A11, 1981.

[11] Giacomo, P.*News from the BIPM.* Metrologia 17, 69 (1981).

[12] J.Burmeister. Specification of the physical and biologically effective absorbed dose in radiation therapies utilizing the boron neutron capture reaction. PhD thesis.Wayne State University,1999.

[13] Loncoln, T., Cosgrove, V., Denis, J.M., Gueulette, J., Mazal, A., Menzel, H.G., Pihet, P. and Sabattier, R. *Radiobiological Effectiveness of Radiation Beams with Broad LET Spectra: Microdosimetric Analysis Using Biological Weighting Functions.* Radiat. Prot. Dosim. 52, 347-352 (1994).

[14] Schröder M. *Characterisation of gas gain of a cylindrical proportional counter at low pressure.* Diploma thesis, Hochschule Aachen, 1996.